Palaeogeography, Palaeoclimatology, Palaeoecology 573 (2021) 110422

Contents lists available at ScienceDirect

Palaeogeography, Palaeoclimatology, Palaeoecology

journal homepage: www.elsevier.com/locate/palaeo

Fossil isotopic constraints (C, O and $^{87}Sr/^{86}Sr$) on Miocene shallow-marine incursions in Amazonia

André Mateus Valentim Alvim [a,*], Roberto Ventura Santos [a], Martin Roddaz [a,b], Pierre-Olivier Antoine [c], Maria Inês Feijó Ramos [d], Dermeval Aparecido do Carmo [a], Ana Paula Linhares [d], Francisco Ricardo Negri [e]

[a] Universidade de Brasília, Darcy Ribeiro Campus, Asa Norte 70910-900 Brasília, DF, Brazil
[b] Géosciences-Environnement Toulouse, Université de Toulouse, UPS (SVT-OMP), CNRS, IRD, 14 Avenue Édouard Belin, F-31400 Toulouse, France
[c] Institut des Sciences de l'Evolution, UMR 5554 CNRS, IRD, EPHE, Université de Montpellier, Place Eugène Bataillon, 34095 Montpellier cedex 5, France
[d] Museu Paraense Emílio Goeldi, Coordenação de Ciências da Terra e Ecologia, Av. Presidente Tancredo Neves 1901, 66077-830 Belém, PA, Brazil
[e] Universidade Federal do Acre, Campus Floresta, Laboratório de Paleontologia. Estrada do Canela Fina, Km 12, 69980-000 Cruzeiro do Sul, AC, Brazil

ARTICLE INFO

Editor: Isabel Patricia Montañez

Keywords:
Amazonian basins
Marine incursions
Pebas Metagawetland system
Miocene fossils
Stable and strontium isotopes
Paleosalinity

ABSTRACT

Several studies have reported Miocene shallow-marine incursions in the Pebas Megawetland system (Western Amazonia) based on paleontological and sedimentological evidence. Only a few publications restricted to Middle and Late Miocene fossils outcropping in the Iquitos (Peru), Benjamin Constant and Eirunepé (Brazil) areas have provided isotopic evidence to test these incursions. In this study, we present new carbon, oxygen, and strontium ($^{87}Sr/^{86}Sr$ ratios) isotopic data of macrofossils (pacu and ray teeth, crab claws and oysters), and microfossils (ostracods and foraminifera) from reported lower to lower upper Miocene sedimentary rocks of Western and Eastern Amazonian (Peru and Brazil), mainly from shallow-marine deposits. It was also analyzed present-day organisms from distinct environments (beach, sea, riverine, and estuary) and compared these results with Miocene fossils. While C and O isotopic compositions indicate that Western Amazonia fossils display an isotopic composition similar to the present-day continental, limnic and riverine, environments (−17‰ to −5.61‰ for $\delta^{13}C$ and − 10.14‰ to −1.92‰ for $\delta^{18}O$), Eastern Amazonia fossils display C and O isotopic compositions comparable to those from seawater environments (−2.53‰ to −0.72‰ for $\delta^{13}C$ and − 4.85‰ to −1.76‰ for $\delta^{18}O$). We further used the $^{87}Sr/^{86}Sr$ isotopic composition of the fossils to estimate paleosalinity conditions. The $^{87}Sr/^{86}Sr$ isotopic compositions indicates that Eastern Amazonian water bodies of the Pirabas Formation (Marajó Basin) varied from mesohaline to marine conditions. In contrast, Early Miocene Western Amazonian water bodies of the Pebas Megawetland System (PMWS) are characterized by freshwater conditions. Nonetheless, in Middle and Early Late Miocene, oligohaline conditions are found in the Peruvian part of the PMWS. Paleosalinity estimates of the Brazilian part of the PMWS are less constrained and might indicate a salinity range between freshwater or oligohaline conditions. Our isotopic data suggest the PMWS was occasionally submitted to oligohaline conditions during Middle and Early Late Miocene shallow-marine incursions. We suggest that Miocene shallow-marine incursions in Western Amazonia at this time were characterized by transitional paleoenvironments, reconciling isotopic, sedimentological and paleontological evidences.

1. Introduction

The number, extent and provenance of Miocene shallow-marine incursions that affected the Western part of Amazonia have received much attention and are still a matter of debate [e.g. (Nuttall, 1990; Hoorn, 1993, 1994; Hoorn et al., 1995; Mathalone and Montoya, 1995; Räsänen et al., 1995; Gingras et al., 2002a; Gingras et al., 2002b; Hermoza, 2004, Hermoza et al., 2005; Rebata et al., 2006; Wesselingh and Macsotay, 2006; Wesselingh et al., 2006; Hovikoski et al., 2007a, 2007b, 2010; Latrubesse et al., 2007, 2010; Hoorn and Wesselingh, 2010; Hoorn et al., 2010; Roddaz et al., 2010; Wesselingh et al., 2010; Rebata, 2012) among many others]). At this time, this area was occupied by the Pebas

* Corresponding author.
E-mail addresses: 200082884@aluno.unb.com (A.M.V. Alvim), rvetura@unb.br (R.V. Santos), martin.roddaz@get.omp.eu (M. Roddaz), pierre-olivier.antoine@umontpellier.fr (P.-O. Antoine), mramos@museu-goeldi.br (M.I.F. Ramos), alinhares@museu-goeldi.br (A.P. Linhares).

https://doi.org/10.1016/j.palaeo.2021.110422
Received 15 June 2020; Received in revised form 13 April 2021; Accepted 19 April 2021
Available online 22 April 2021
0031-0182/© 2021 Elsevier B.V. All rights reserved.

Megawetland system, a long-lived wetland formed by a complex mosaic of swamps, lakes and fluvial systems influenced by marine incursions episodes (Early to Early Late Miocene) and the riverine, locally lacustrine, Acre systems (Late Miocene; Hoorn et al., 2010; Marivaux et al., 2020). Recent studies suggest the occurrence of three shallow-marine incursions within Western Amazonia during Miocene times: i) one Early Miocene incursion between 18.1 and 17.2 Ma, expanding through Venezuelan and Colombian basins to the Solimões Basin (e.g. Dueñas-Jimenez, 1980; Hoorn, 1990, 1993, 1994; Rull, 2001; Gómez et al., 2005; Parra et al., 2009; Linhares et al., 2011; Villegas et al., 2016; Jaramillo et al., 2017; Linhares et al., 2017); ii) one Middle Miocene incursion between 16.1 and 12.4 Ma, expanding through Venezuelan and Colombian basins to the Ucayali Basin and the Solimões Basin (e.g. Hoorn, 1990, 1993, 1994; Monsch, 1998; Vonhof et al., 1998, 2003; Wesselingh et al., 2002; Salas-Gismondi et al., 2006, 2007; Antoine et al., 2007, 2016; Bayona et al., 2007; Dueñas-Jimenez and van der Hammen, 2007; Gross et al., 2014, 2015; Jaramillo et al., 2011; Boonstra et al., 2015; Chabain et al., 2017; Jaramillo et al., 2017; Medeiros et al., 2019); iii) one Late to Middle/Early Late Miocene incursion between 12 and 10 Ma, approximately, expanding through Ecuadorian, Peruvian, Bolivian and Brazilian basins (e.g. Tschopp, 1953; Nicolaidis and Coimbra, 2008; Uba et al., 2009; Hoorn and Wesselingh, 2010; Linhares et al., 2011; Salas-Gismondi et al., 2015; Antoine et al., 2016; Chabain et al., 2017; Linhares et al., 2017; Kern et al., 2020). There is only one Early Miocene marine incursion recorded within Eastern Amazonia in the Pirabas Formation of the Brazilian Marajó Basin (e.g. Petri, 1957; Fernandes, 1984; Góes et al., 1990; Rossetti and Santos Jr., 2004; Rossetti, 2006; Zalán and Matsuda, 2007; Távora et al., 2014; Ferreira, 2015; Nogueira et al., 2019).

Shallow-marine incursions in the Amazonian sedimentary basins have been identified mainly based on the presence of marine and brackish water fossils (e.g., dinoflagellates, pollens and benthic foraminifera, fishes [selachians]), bioturbations, and tidal structures (see Hovikoski et al., 2010; Boonstra et al., 2015, and references therein). In the Brazilian intracratonic basins, such as the Solimões Basin, the only piece of evidence is based on fossils, and no tidal structures have been identified so far (Gross et al., 2011; Gross et al., 2013; Linhares et al., 2011, 2017; Medeiros et al., 2019).

Besides these evidences, geochemical proxies, such as stable and radiogenic isotopes, may also be powerful tools to identify marine influences in continental areas. For instance, oxygen isotopic ratio in water can vary by mixing two sources with distinct $^{18}O/^{16}O$ signatures (freshwater and seawater for example), and some contribution from evaporation processes (Bigg and Rohling, 2000). The carbon isotopes of dissolved inorganic carbon (DIC) in coastal to estuarine settings can have a direct relationship with water salinity, especially above 25 psu (Mook and Vogel, 1968; Fry, 2002; Bouillon et al., 2011). In contrast to stable isotopes, the $^{87}Sr/^{86}Sr$ isotopic compositions of carbonate fossils are neither altered by evaporation/precipitation nor by biological processes (Schmitz et al., 1991; Bryant et al., 2015). Therefore, fossil $^{87}Sr/^{86}Sr$ ratios may be used as a proxy indicator of salinities of modern and ancient brackish-water systems (Ingram and DePaolo, 1993; Bryant et al., 1995; Holmden et al., 1997; Spencer and Patchett, 1997; Vonhof et al., 1998, 2003). In Western Amazonia, paleosalinity estimates based on the strontium isotopic composition of mollusk shells indicate a predominantly freshwater environment, but also reveal the rare presence of mesohaline and oligohaline waters within the Pebas Megawetland associated with the presence of a more saline molluscan faunal assemblage (Vonhof et al., 1998, 2003). Although restricted to a local area, these pioneering studies have shown the utility of these isotopic proxies for detecting and characterizing the salinity of Amazonian paleoenvironmental depositional systems.

This study aims to provide C, O and $^{87}Sr/^{86}Sr$ isotopic data of fossils recovered from Miocene sedimentary sequences that shallow-marine incursions were reported in Western and Eastern Amazonia. We analyze a wide array of macro- and microfossils of presumably Miocene shallow-marine intervals from sedimentary basins of the Peruvian and Brazilian Amazonia. We discuss whether these isotope data may be reconciled with the sedimentological and paleontological evidence for marine incursions presented in previous studies (Fig. 1).

2. Material and methods

2.1. Material

One hundred and five samples were selected from diverse shallow-marine, and few non-marine, intervals from Western Amazonia (Peru and Brazil) and Eastern Amazonia (Brazil) for $\delta^{13}C$, $\delta^{18}O$, and $^{87}Sr/^{86}Sr$ analyses (Table S1; Figs. 2 and 3). In these samples, we have analyzed 374 fossil specimens. As a complimentary database, Table 1 shows the salinity ranges in which the most representative fossil groups are assigned to live in their habitat.

2.1.1. Early to Early Late Miocene (23–11 Ma)

Twenty-one Early Miocene fossil specimens were selected for isotope analysis, among which 13 were collected from marine sequences of the Pirabas Formation in Marajó Basin at Atalaia Beach and Capanema areas (Pará State, Brazil) by the authors. In detail, five foraminifera tests (*Amphistegena*), one crab claw and two ray teeth (*Myliobatis*) come from Atalaia Beach. One urchin and four manatee vertebrae fragments come from Capanema. Also, eight Early Miocene pacu teeth were collected from the Pebas Formation in the Ucayali Basin at CTA-63 locality (Contamana area, Peru; Antoine et al. (2016).

Ninety-four Middle Miocene fossil specimens were selected for isotope analysis. Overall, 56 *Cyprideis* ostracod shells and 18 *Ammonia* and *Elphidium* foraminifera tests were recovered from the Solimões Formation (well 1-AS-33 AM) by Medeiros et al. (2019). For the sake of comparison, 44 ostracods were taken from non-marine intervals (106.65 m, 147.4 m, 156.8 m, 157.35 m, 260.05 m and 290.05 m depths), and 12 ostracods and 18 foraminifera were taken from reported marine incursion intervals (136.35 m and 139.4 m depths). Moreover, four crab claws and eight pacu teeth were collected from a reported marine interval of the Ipururo Formation in the Huallaga Basin at the outcrop TAR-31 (Tarapoto area, Peru; ~13.1–12.6 Ma; Marivaux et al., 2020). In addition, eight pacu teeth were collected from a reported marine interval of the Pebas Formation in the Ucayali Basin at CTA-45 locality (Contamana area, Peru; Antoine et al., 2016).

Finally, for the lower upper Miocene interval (~12–9 Ma), 253 fossil specimens were selected for isotope analyses. Among these specimens, 14 *Cyprideis* shells, 14 *Ammonia* tests, four gastropod shells, and three charophytes oogonia were analyzed from reported marine (110.2 m

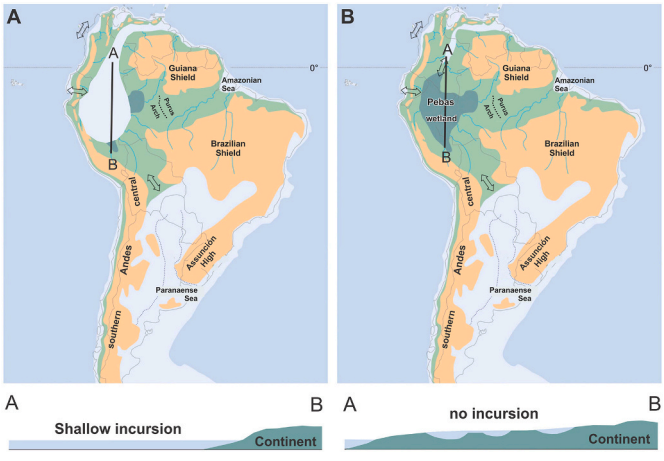


Fig. 1. Paleogeographical hypothesis for the marine incursions intervals, using the scenario of the Amazonia Basin during Miocene as background (adapted from Gross et al., 2015).

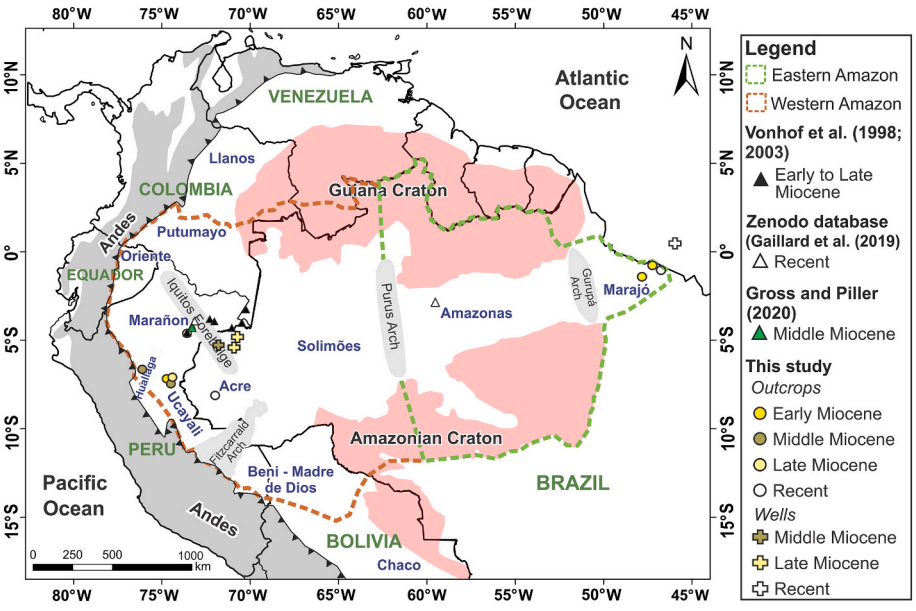


Fig. 2. Location of the analyzed fossil samples classified by the time of the Miocene marine incursion occurrences within the Amazonian Basin. Structural archs and forebulge positions and ranges are defined according to Roddaz et al. (2005) and Espurt et al. (2007).

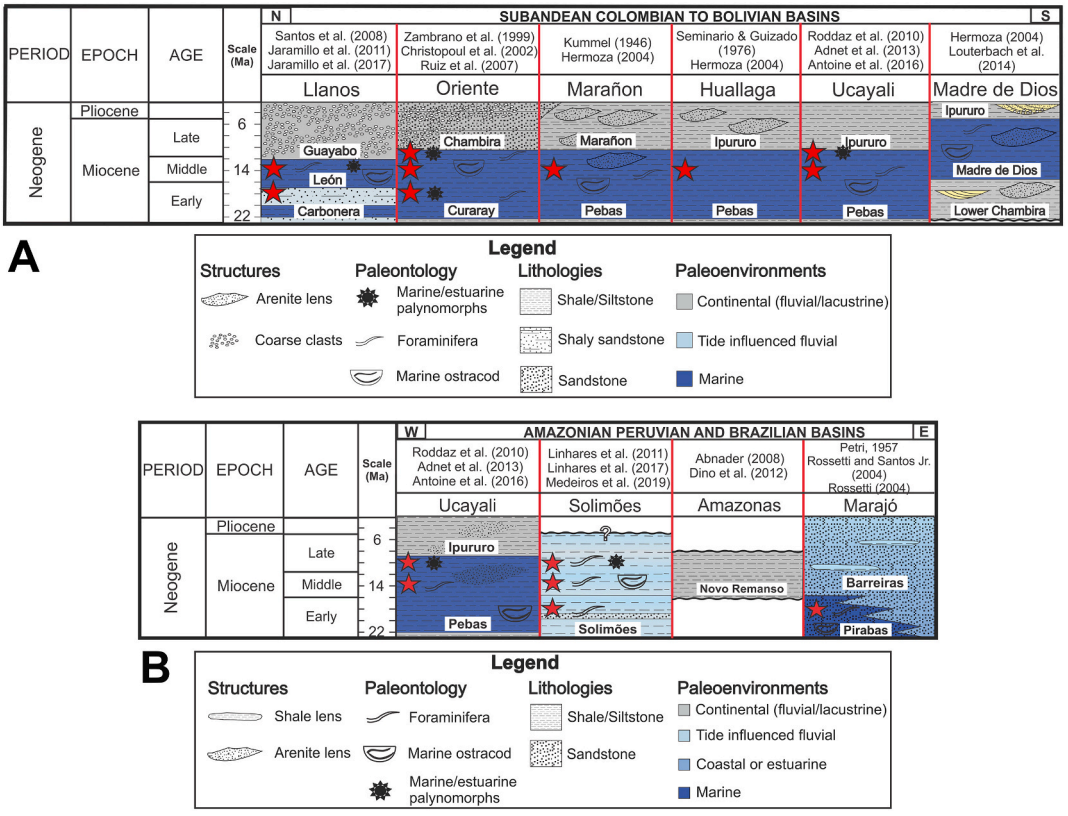


Fig. 3. Simplified North-South (A) and East-West (B) chronostratigraphic charts for the Amazonian Basin. Red stars mark the marine incursions described in text. (For interpretation of the references to colour in this figure legend, the reader is referred to the web version of this article.)

depth of the 1-AS-5 AM well and 73.6 m depth of the 1-AS-7D AM well) and non-marine (50.0 m and 115.5 m depths of the 1-AS-7D AM well) intervals of the Solimões Formation (Ana Paula Linhares [Pers. Com.] and Linhares et al., 2017, 2019, respectively). Other 11 pacu teeth, 24 *Pristis* teeth, two crab claws, two *Crassostrea* oysters and 165 *Ammonia* foraminifera tests were recovered from previously reported marine intervals of the Pebas Formation in the Ucayali Basin at CTA-43 (Lower Upper Miocene), CTA-44top, CTA-58 and CTA-77 (transition between Middle and Late Miocene), and CTA-43 (lower upper Miocene) localities in the Contamana area, Peru (Antoine et al., 2016). Finally, three *Cyprideis* ostracod shells, three *Hydrobiidae* mollusks shells and five *Ammonia* foraminifera tests were analyzed from a reported marine interval of the Pebas Formation in the Marañon Basin (Nuevo Horizonte area, Peru; Wesselingh et al., 2002).

Table 1
Most representative fossil groups analyzed in this study and their respective salinity tolerance and bathynetry range. Observe that most of those groups lived in distinct environments and could adapt to salinity levels below seawater.

Fossil Group	Genera	Range of salinity tolerance	Bathymetry range (m)	Bibliography
Ostracoda	*Cyprideis*	High, freshwater to hypersaline (0–40 psu approximately)	0–30	Coimbra et al. (2007); Boomer et al. (2016); Meyer et al. (2017)
Foraminifera	*Ammonia*	High, slightly oligohaline to hypersaline (1–70 psu approximately)	0–50	Murray (1991); Hohenegger et al. (1993); Murray (2006); Gross and Piller (2020)
	Elphidium	High, slightly oligohaline to hypersaline (1–70 psu approximately)	0–50	Murray (1991, 2006); Hohenegger et al. (1993); Chappell and Wang (2001); Gross and Piller (2020)
	Amphistegina	Low, marine (coral reefs and lagoons; usually higher than 34 psu)	0–130	Zmiri et al. (1974); Murray (1991); Murray (2006)
Bony fish	Pacu (serrasalmines family)	Low, freshwater to mesohaline waters (0–10 psu approximately)	0–10	Barbosa Júnior et al. (2010); Souza-Bastos et al. (2016)
Rays	*Myliobatis* (eagle ray)	High, freshwater (less common) to estuarine and marine	0–20	McEachran and Aschliman (2004); Cousseau et al. (2007)
	Pristis (saw-fish)	High, slightly oligohaline to marine (including coastal areas, estuaries and swamps; 1–41 psu)	0–20	Stevens et al. (2008); Thorburn et al. (2008)
Crabs	Trichodactylidae family (freshwater crabs)	Freshwater to polyhaline waters (0–21 psu)	0–2	Magalhães (1999); Yeo et al. (2008); Firmino (2009); Klaus et al. (2017)
Charophytes	*Stephanochara*	Freshwater to polyhaline waters (0–20 psu)	0–10	Blindow (2000); Sanjuan and Martín-Closas (2012)

2.1.2. Recent

Thirteen recent specimens were retrieved from in distinct Amazonian sites (Table S1). In details, samples from Eastern Amazonia comprise three frog bones and three crab shells (originated from an owl regurgitation), and two oysters (*Crassostrea sp.*) from Atalaia Beach and Mosqueiro Island; and 4 foraminifera tests (*Amphistegina*) from a well of the Piatam Ocean Project, located 150 km away from the coast. Samples from the Western Amazonia include a trichodactylid crab claw from a bank of the Tarauacá River at the Acre State (Brazil).

2.2. Stable isotopes (C and O) and Fe-Mn concentrations

Most of macrofossil sample preparation includes cleaning with methanol and ultrasonic waves (Boyle, 1981; Rosenthal et al., 1999) to remove adherent clays onto their surfaces, and pulverization of larger macrofossils (as urchins and crab claws) with a drill or fragmentation of smaller macrofossils (as ray and fish teeth) with an agate mortar to obtain 5–10 mg powder aliquots (one per sample). Each aliquot is the result of pulverization or fragmentation of one or more specimens of the same fossil species (Table S2). For oysters from outcrops CTA-58 and CTA-77 (Contamana area), we used a microdrill to take aliquots of the same specimen along the shells' growth lines and away from the umbos (5 mm spacing). For microfossil samples, we handpicked the cleanest specimens by stereo microscope evaluation (Zeiss Stemi 508).

The macrofossil samples were analyzed at the Geochronology Laboratory of the University of Brasília on a Delta V Plus mass spectrometer connected to a Gas Bench II apparatus. Samples reacted with H_3PO_4 at a temperature of 72 °C after flushing the flask using helium flow. Stable isotope results are reported in delta notation relative to the Vienna Pee Dee Belemnite reference standard (V-PDB) and were calibrated against NBS 18 ($\delta^{13}C_{V\text{-}PDB} = -5.01‰$ and $\delta^{18}O_{V\text{-}PDB} = -23.2‰$) and NBS 19 ($\delta^{13}C_{V\text{-}PDB} = 1.95‰$ and $\delta^{18}O_{V\text{-}PDB} = -2.20‰$) standards. Repeated analyses of the NBS 18 standard gave −5.32‰ ± 0.09 for $\delta^{13}C$ and − 23.68 ± 0.1 for $\delta^{18}O$ (SD, $n = 40$) close to the recommended value. Linear regression of the standard results followed by correction of the samples data were made to account for instrumental bias. Data uncertainty (SD) varies from ±0.01‰ to ±0.28‰ for $\delta^{13}C$ and from ±0.01‰ to ±0.12‰ for $\delta^{18}O$.

Microfossils were analyzed at the Geochronology Laboratory of the University of Brasília on a MAT 253 mass spectrometer connected to a Kiel IV Carbonate device. Within Kiel IV the samples reacted with H_3PO_4 at a temperature of 70 °C and the CO_2 generated by this reaction went through a two-phase cryogenic trapping system that filters H_2O and other gases and leads the CO_2 to the mass spectrometer. The results are reported in delta notation relative to the Vienna Pee Dee Belemnite reference standard (V-PDB) and were calibrated against NBS-18 and NBS-19 standards and Rei-1 ($\delta^{13}C_{V\text{-}PDB} = -7.85‰$ and $\delta^{18}O_{V\text{-}PDB} = -7.90‰$), OC-1 ($\delta^{13}C_{V\text{-}PDB} = 2.49‰$ and $\delta^{18}O_{V\text{-}PDB} = -2.40‰$) and CABRA ($\delta^{13}C_{V\text{-}PDB} = 2.00‰$ and $\delta^{18}O_{V\text{-}PDB} = -5.00‰$) internal standards. Repeated analyses of the NBS 18 standard gave −4.81 ± 0.08 for $\delta^{13}C$ and − 22.70 ± 0.42 for $\delta^{18}O$ (SD, $n = 10$). Linear regression of the standard results followed by correction of the samples data indicated that their uncertainty (SD) varies from 0.01‰ to 0.25‰ for $\delta^{13}C$ and from 0.02‰ to 0.21‰ for $\delta^{18}O$.

The residual solution obtained from the stable isotope analysis (solution of the sample after H_3PO_4 attack), of 32 samples from Brazilian and Peruvian Western Amazonian sites were used to determine their concentrations of Fe and Mn (samples 10–12, 14–27, 28–29, 31–36, 94–99; Table S2). The residual material of each sample was attacked with HNO_3 (2.5 M) in distinct Savilex digestion vessels and diluted in MilliQ water (factor of dilution = 7) within 15 mL conical tubes. Afterward, Fe and Mn contents were determined by OES-ICP- (5100 Agilent, USA) at the Geochemistry Laboratory of the University of Brasília. ICP-OES detection limits are set as 2 μg/L for Mn and 10 μg/L for Fe. The relative standard deviation of the Fe and Mn concentrations varies from 10 to 11% for Fe and 8 to 9% for Mn data.

2.3. $^{87}Sr/^{86}Sr$ isotopic composition

Thirty-five $^{87}Sr/^{86}Sr$ measurements were obtained in fossils and modern organisms from Amazonia. In most instances, we have used more than one specimen for each analysis. Among the 35 analyzed aliquots, 31 also have $\delta^{13}C$ and $\delta^{18}O$ isotopic compositions. The macrofossil samples were previously cleaned with methanol and ultrasonic waves (Boyle, 1981; Rosenthal et al., 1999) to remove adherent clays onto their surfaces. The measurement of $^{87}Sr/^{86}Sr$ ratios followed two different procedures: one based on 20-mg aliquot macrofossil powder; and another based on the residual solution taken after $\delta^{13}C$ and $\delta^{18}O$ analysis, when possible. Regarding the first methodology, after powdering, an aliquot of 20 mg was weighed in cleaned Savillex PFA vials and then digested with 2 mL of acetic acid (CH_3COOH; 0.5 N) to remove only the carbonate fraction and avoid leaching of ^{87}Rb and radiogenic ^{87}Sr from the non-carbonate constituents. Then, a sequence of ultrasonic bath for 20 min, centrifugation for 10 min, supernatant retrieve (1 mL), evaporation in a hot plate (60 °C), and finally, dissolution in 1 mL HNO_3 (2,9 N) was done for each sample before loading into ionic exchange columns. Regarding the second methodology, residual solution from $\delta^{13}C$ and $\delta^{18}O$ analysis were digested with 1 mL of HNO_3 (2.9 N) for 24 h and then, loaded into exchange columns. Concentrated Sr solutions were obtained after ion chromatography

using an ion exchange resin Sr-spec. Blank tests performed to estimate the level of contamination induced by the acid digestion were found to be negligible. The $^{87}Sr/^{86}Sr$ ratios were then measured using a Neptune Thermo MC-ICP-MS at Geochronology Laboratory of the University of Brasília. The measurements were calibrated against NBS 987 standard (= 0.710240; Hodell et al., 2007). Repeated analyses of the NBS 987 standard gave an $^{87}Sr/^{86}Sr$ ratio of 0.71028 ± 0.000020 (2SD, $n = 40$) in agreement with the recommended value of Hodell et al. (2007), therefore no instrumental bias needs to be taken into account.

2.4. Statistical methods

Statistical methods, such as ANOVA one-way and *t*-tests for instance, were applied to our results using the software RStudio version 1.3.1093 (RStudio Team, 2020) in order to evaluate changes in the variability of the carbon and oxygen isotopic data of the analyzed samples.

2.5. Paleosalinity calculations

Paleosalinity estimates based on fossil Sr isotopic composition followed the methodology developed in Vonhof et al. (1998, 2003). For Western Amazonia, paleosalinity estimates were calculated through standard binary-mixing models (Eq. (1); Vonhof et al., 1998, 2003) using three end members with distinct isotopic compositions: Miocene seawater, cratonic runoff, and Andean runoff.

$$^{87}Sr/^{86}Sr_m = \left\{ \left(^{87}Sr/^{86}Sr_a \text{ x } [Sr]_a \text{ x } A + {}^{87}Sr/^{86}Sr_b \text{ x } [Sr]_b \text{ x } B \right) \right\} \div \left\{ \left(A \text{ x } [Sr]_a + B \text{ x } [Sr]_b \right) \right\} \quad (1)$$

Eq. (1). Equation, based in Vonhof et al. (1998, 2003), for construction of binary-mixing models using the Sr concentrations and $^{87}Sr/^{86}Sr$ isotopic ratios of the end members cited in the text.

In Eq. (1), $^{87}Sr/^{86}Sr_m$ is the Sr isotopic ratio of a mixture of two end members, $^{87}Sr/^{86}Sr_a$ and $^{87}Sr/^{86}Sr_b$ are the Sr isotopic ratios of each end member, $[Sr]_a$ and $[Sr]_b$ are the Sr concentrations of each end member, and A and B are the relative proportions of each end member in the mixture (A + B = 1). Regarding the end members' Sr parameters, Sr concentration and $^{87}Sr/^{86}Sr$ ratios of the Miocene seawater end member are the same as in Vonhof et al., 1998, 2003; (Table 2). For the cratonic and Andean runoff end members, we used the data from Vonhof et al. (1998) and other data from modern Amazon Basin rivers (Allègre et al., 1996; Santos et al., 2014; Table 2).

Based on these models, we made water mixing curves diagrams and $^{87}Sr/^{86}Sr$ vs seawater content (or salinity) cross plots. The interception between the $^{87}Sr/^{86}Sr$ ratios of the analyzed samples and mixing curves defines seawater content and paleosalinity estimates. Freshwater and oligohaline-water salinity curves (0.5 and 5 psu) were calculated utilizing the previous binary-mixing models and calibrated with a seawater salinity curve (Howarth and McArthur, 1997).

3. Results

This section presents the geochemical results of the analyzed samples according to the chronological order of the reported shallow-marine incursions (Table S2). For comparison, we present stable isotopic results together with carbon and oxygen isotope ranges of modern mollusks from North America rivers, Great Lakes, and North Atlantic Seawater, the Black Sea and the San Francisco Bay estuary (Keith et al., 1964; Ingram et al., 1996; Logvina et al., 2004; Varol, 2015), as well as Miocene stable isotopic data from Vonhof et al. (1998, 2003), and Gross and Piller (2020) and Recent data from Gaillard et al. (2019). Although we use modern parameters from localities distinct from our sampling sites, the isotopic fractionation processes in those environments are likely to have occurred in the most common environments of the Pebas Megawetland System as well (e.g. lakes, rivers and swamps).

We also present $^{87}Sr/^{86}Sr$ isotopic ratios together with Miocene $^{87}Sr/^{86}Sr$ isotopic ratios measured in Vonhof et al. (2003). Ages of Buenos Aires, Porvenir, Nuevo Horizonte and Los Chorros outcrops were updated according to Boonstra et al. (2015) and Gross and Piller (2020).

3.1. Recent

Carbon and oxygen isotopic data from Recent specimens range from −16.87‰ to −0.07‰, and − 8.01‰ to −0.12‰, respectively (Fig. 4A; Table S2). Overall, there are two distinct data populations. The first one comprises the mollusks sampled at the Brazilian and Peruvian Amazon rivers (Zenodo database; Gaillard et al., 2019), crab claws and frog bones sampled at Pará State (Brazil) mangroves, crab claws sampled at Acre State (Brazil) rivers and an oyster sampled at Mosqueiro Island (estuary environment; Silva, 1975; Venturieri et al., 1998). These samples present carbon isotope values ranging between −16.99‰ and − 9.81‰, and oxygen isotopes values between −8.01‰ and − 1.31‰. The Peruvian river mollusks and both riverine and mangrove crab claws present lower $\delta^{18}O$ values than the Brazilian river mollusks and the estuarine oyster. The second data population comprises the foraminifera (*Amphistegina*) sampled in the Equatorial Atlantic Ocean and the oyster (*Crassostrea*) sampled at Atalaia beach. These samples present less negative $\delta^{13}C$ and $\delta^{18}O$ values, closer to those of the North Atlantic seawater range (Fig. 4A; Table S2).

Table 2
$^{87}Sr/^{86}Sr$ ratios and Sr concentrations of seawater in Early Miocene (Psiladiporites zone), Middle Miocene (Crassoretitriletes zone) and Late Miocene (Grimsdalea zone) times (Howarth and McArthur, 1997), and present-day rivers (Palmer and Edmond, 1992) used by Vonhof et al. (1998, 2003) (left side). Same data from Santos et al. (2014) with cratonic freshwater and catchments data contribution from Allègre et al. (1996) (right side).

Vonhof et al. (1998, 2003)			Santos et al. (2014)		
			Allègre et al. (1996)		
End members	$^{87}Sr/^{86}Sr$	Sr (ppm)	End members	$^{87}Sr/^{86}Sr$	Sr (ppm)
Seawater *Grimsdalea* zone	0.70886	7.886	Seawater *Grimsdalea* zone	0.70887	7.886
Seawater *Crassoretitriletes* zone	0.70876	7.886	Seawater *Crassoretitriletes* zone	0.70877	7.886
Seawater *Psiladiporites* zone	0.70855	7.886	Seawater *Psiladiporites* zone	0.70855	7.886
Cratonic freshwater	0.7282	0.0107	Cratonic freshwater	0.73072	75
Andean freshwater	0.7074	0.0416	Andean freshwater	0.70868	0.1713
Napo River	0.7059	0.0416	Napo River	0.70592	0.0515
Catchments	$^{87}Sr/^{86}Sr$	Sr (ppm)	Catchments	$^{87}Sr/^{86}Sr$	Sr (ppm)
Andean catchments					
Madeira subbasin	0.7188	0.098	Madeira subbasin	0.71677	0.098
Ucayali-Maranon subbasin	0.7093	0.235	Ucayali-Maranon subbasin	0.70887	0.279
Northern Andes subbasin	0.7074	0.0291	Northern Andes subbasin	0.7074	0.0291
Cratonic catchments					
Guyana craton rivers	0.7266	0.0103	Guyana craton rivers	0.73072	75
Brazilian craton rivers	0.7307	0.0112	Brazilian craton rivers	0.74496	75

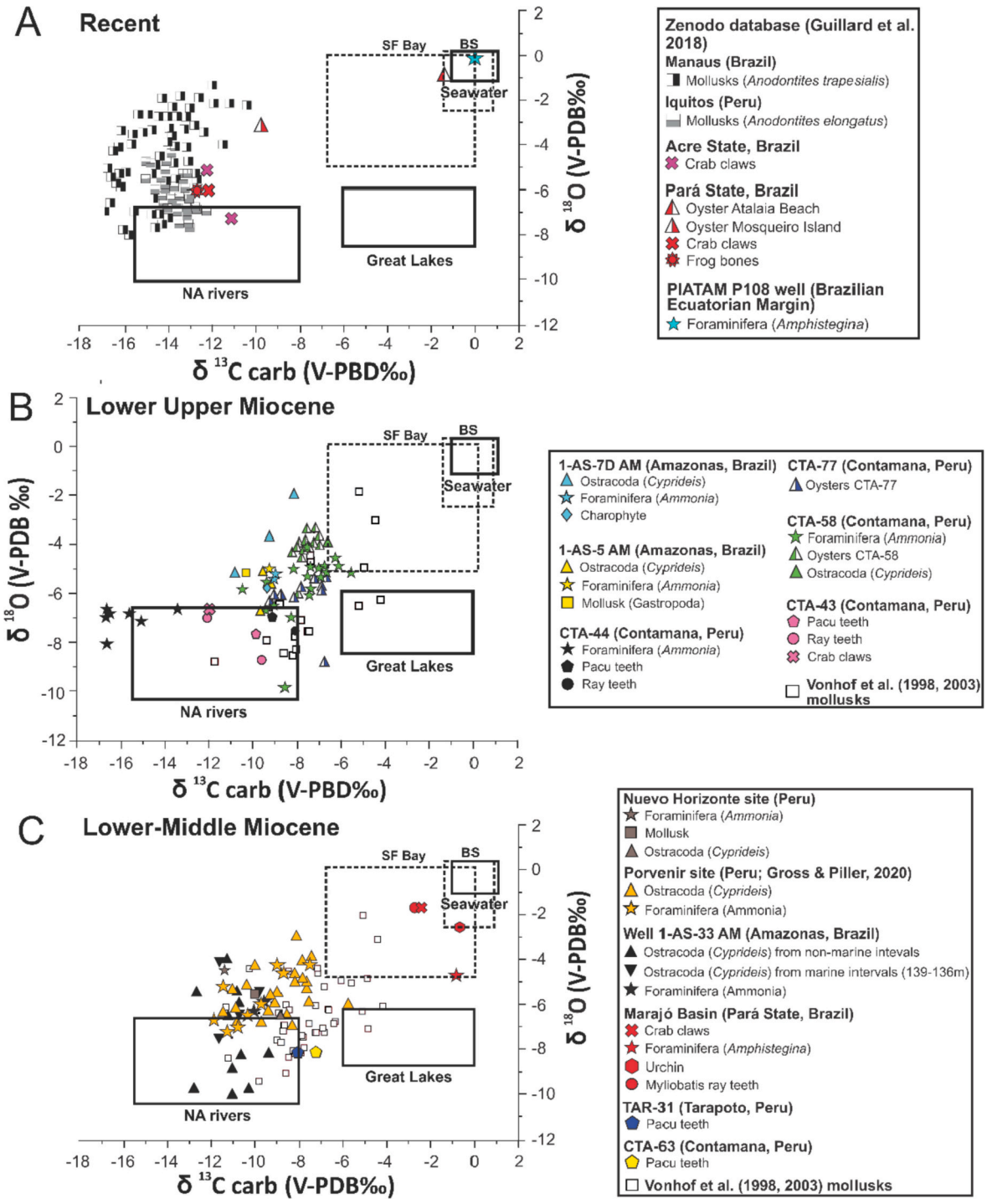


Fig. 4. Carbon versus oxygen isotopes cross plot of lower to Middle Miocene (C), lower upper Miocene (B) and Recent (A) fossil samples. Black boxes represent standard stable isotopes values of modern mollusks from North Atlantic seawater, Great Lakes, and North American rivers (Keith et al., 1964), the San Francisco Bay estuary (Ingram et al., 1996) and the Black Sea (Logvina et al., 2004; Varol, 2015).

3.2. Early to Middle Miocene (23–12.1 Ma)

Carbon and oxygen isotopic data of Early and Middle Miocene fossil samples present two data populations. The first group comprises fossils from the Pebas Megawetland System (well 1AS-1S-33AM from the Brazilian Amazonas Basin, and outcrops TAR-31, CTA-63 and Nuevo Horizonte from the Peruvian Amazon) and exhibits $\delta^{13}C$ values between −12.78‰ and − 7.21‰, and $\delta^{18}O$ between −10.13‰ and − 4.07‰ (Fig. 4C; Table S2). These data are similar to the most negative $\delta^{13}C$ and $\delta^{18}O$ values of the mollusks analyzed by Vonhof et al. (1998, 2003) and the ostracods and foraminifera analyzed by Gross and Piller (2020), which are close or within the North American river interval (Fig. 4C). The $\delta^{13}C$ and $\delta^{18}O$ data of foraminifera and ostracods from marine incursion intervals of the well 1-AS-33-AM plot in the same range as the ostracods from non-marine intervals. The second data population consists of $\delta^{13}C$ and $\delta^{18}O$ values of Early Miocene samples from the Pirabas Formation (Marajó Basin at Eastern Amazonia). They yield less negative $\delta^{13}C$ and $\delta^{18}O$ values, which plot close to the North Atlantic seawater and within the San Francisco estuary intervals (Fig. 4C).

$^{87}Sr/^{86}Sr$ isotopic ratios of Early Miocene fossils are variable and

range from 0.70759 to 0.70885 (Fig. 5; Table S2). Samples from Peruvian Western Amazonia (Contamana area) have $^{87}Sr/^{86}Sr$ compositions that range between 0.70759 and 0.70771, being slightly less radiogenic than those of Indiana outcrop of Vonhof et al. (2003). Samples from the Pirabas Formation (Marajo Basin), exhibit more radiogenic $^{87}Sr/^{86}Sr$ isotopic ratios, ranging between 0.70866 and 0.70885 (Fig. 5).

The Middle Miocene fossils from the Peruvian Western Amazonia (Contamana and Tarapoto areas), yield a narrow range of $^{87}Sr/^{86}Sr$ ratios between 0.70771 and 0.70819, similar to those of Santa Rosa/Pebas and Los Chorros/Nuevo Horizonte/Porvenir of Vonhof et al. (2003) (Fig. 5). The Middle Miocene fossils from the Brazilian Western Amazonia (well 1-AS-33-AM) present a wide range of $^{87}Sr/^{86}Sr$ isotopic ratio between 0.70607 and 0.73424 (Fig. 5).

3.3. Earliest Late Miocene (11.9–11 Ma)

Carbon and oxygen isotopic data of earliest Late Miocene fossils from Brazilian and Peruvian Amazon basins range from −16.76‰ to −5.61‰, and − 9.71‰ to −1.92‰, respectively (Fig. 4B; Table S2). Overall, they plot between the North American river and the Great Lakes boxes, similar to those from Early/Middle Miocene fossils of Western Amazonia, but closer to the San Francisco estuary interval (Fig. 4B). However, there is a distinct population of foraminifera (*Ammonia*) from the Peruvian Amazon (CTA-44 outcrop) that presents more negative $\delta^{13}C$ values (between −13.51‰ and − 16.76‰; Fig. 4B).

The analyzed fossil samples from Peruvian Western Amazonia (Contamana area), yield $^{87}Sr/^{86}Sr$ isotopic ratios ranging between 0.70778 and 0. 0.70861 (Fig. 5; Table S2). They plot within the Santa Rosa/Pebas box to slightly above the Los Chorros/Nuevo Horizonte /Porvenir box of Vonhof et al. (2003); Fig. 5). The Middle Miocene fossils from the Brazilian Western Amazonia (wells 1-AS-7D-AM and 1-AS-5-AM) present a wider range of $^{87}Sr/^{86}Sr$ (0.70802 and 0.71026; Fig. 5).

4. Paleosalinity estimate based on $^{87}Sr/^{86}Sr$ isotopic ratio

The potential end members for the calculation of binary-mixing models include Andean rivers, cratonic rivers and seawater (henceforth called by A, C and S respectively). For the Early to Early Late Miocene Peruvian Western Amazonian samples (Ucayali and Huallaga Basins, Contamana and Tarapoto areas respectively), a binary mixture between seawater and Andean rivers (S-A model) is the most likely scenario. We envisage no contribution of cratonic rivers in the area is expected, since sediments in the North Amazonian retroarc foreland basins had already an Andean provenance during Miocene times (Roddaz et al., 2005; Villegas et al., 2016; Louterbach et al., 2017; Hurtado et al., 2018). Mixing models using $^{87}Sr/^{86}Sr$ isotopic composition of the analyzed Peruvian Amazonian samples suggest that paleosalinity varied between 0.17 and 3.15 psu, which corresponds to 0.5–9% of seawater content (Supplementary Datafile 1, Table 3). In details, samples 1 and 7 (pacu teeth) indicate freshwater conditions, while samples 8, 9, 28, 37, 38, 39, 40, 48, 49 and 94 (other pacu teeth, mollusks, *Pristis* teeth, crab claws and *Cyprideis* ostracod) indicate oligohaline waters (Fig. 6; Table 3).

For the Early to Middle Miocene Brazilian Western Amazonian samples (1-AS-33-AM, 1-AS-5-AM and 1-AS-7D-AM wells), three alternative binary mixtures are possible: seawater and Andean rivers (S-A model), seawater and cratonic rivers (S—C model), and Andean and cratonic rivers (A-C model). This occurs because Neogene sedimentary rocks of the Brazilian Amazonian retroarc foreland basin system are located to the east of the Iquitos forebulge, and may be either sourced by Andean or cratonic paleodrainage system (Roddaz et al., 2005; Roddaz et al., 2006; Horbe et al., 2019). The different mixing models are detailed below:

i. Seawater and Andean rivers mixing models were applied to samples that yielded $^{87}Sr/^{86}Sr$ isotopic compositions below the $^{87}Sr/^{86}Sr$ ratios of Middle (0. 70,876) and Early Late Miocene

Size suggestion: two columns

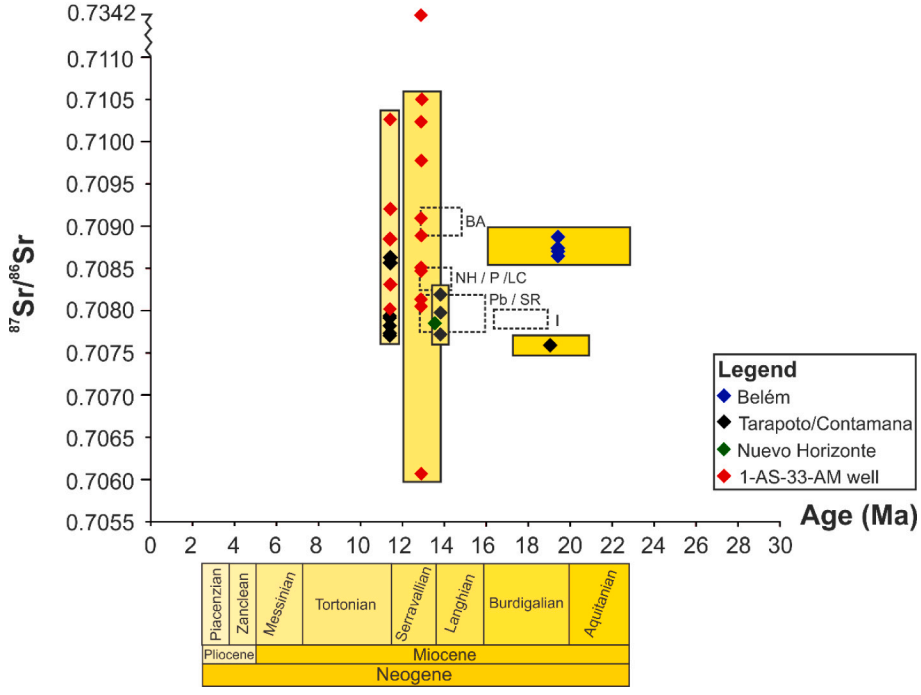


Fig. 5. $^{87}Sr/^{86}Sr$ ratio vs age crossplot for lower Miocene, Middle Miocene and lower upper Miocene Amazonian fossil samples from Contamana and Tarapoto, 1-AS-33-AM well, Nuevo Horizonte and Belém sites with their respective full stratigraphic range. Dashed boxes represent molluskcan data from Vonhof et al. (2003) for the following Peruvian sites: Indiana (I), Pebas (Pb), Santa Rosa (SR), Los Chorros (LC), Porvenir (P), Nuevo Horizonte (NH) and Buenos Aires (BA).

Table 3
Paleosalinity estimation, % of seawater content or % of Andean vs Cratonic water content based on binary mixing calculations of the $^{87}Sr/^{86}Sr$ isotopic composition of analyzed sample.

Samples	$^{87}Sr/^{86}Sr$	Binary mixing model							
		Andean waters vs Seawater			Cratonic water vs Seawater			Andean water vs Cratonic water	
		PSU	% Seawater	Interpretation	PSU	% Seawater	Interpretation	%Andean	% Cratonic
Peruvian Western Amazonian basins									
1 (pacu teeth)	0.70759	0.17	0.5	Freshwater	N.C.	N.C.	N.C.	N.C.	N.C.
7 (pacu teeth)	0.70771	0.48	1.37	Freshwater	N.C.	N.C.	N.C.	N.C.	N.C.
28 (mollusks)	0.70785	0.6	1.8	Oligohaline	N.C.	N.C.	N.C.	N.C.	N.C.
37 (ray teeth)	0.70778	0.52	1.5	Oligohaline	N.C.	N.C.	N.C.	N.C.	N.C.
40 (*Pristis* ray teeth)	0.70779	0.6	1.8	Oligohaline	N.C.	N.C.	N.C.	N.C.	N.C.
8 (crab claws)	0.70797	1.05	3	Oligohaline	N.C.	N.C.	N.C.	N.C.	N.C.
9 (pacu teeth)	0.70819	1.4	4	Oligohaline	N.C.	N.C.	N.C.	N.C.	N.C.
38 (crab claws)	0.70856	2.8	8	Oligohaline	N.C.	N.C.	N.C.	N.C.	N.C.
39 (pacu teeth)	0.70795	1.05	3	Oligohaline	N.C.	N.C.	N.C.	N.C.	N.C.
48 (*Pristis* ray teeth)	0.70787	0.87	2.5	Oligohaline	N.C.	N.C.	N.C.	N.C.	N.C.
49 (pacu teeth)	0.70798	1.22	3.5	Oligohaline	N.C.	N.C.	N.C.	N.C.	N.C.
94 (*Cyprideis* ostracod)	0.70861	3.15	9	Oligohaline	N.C.	N.C.	N.C.	N.C.	N.C.
Brazilian Western Amazonian basins									
20 (*Cyprideis* ostracod)	0.70607	0	0	Freshwater	N.C.	N.C.	N.C.	100	0
15 (*Cyprideis*ostracod)	0.70848	2.27	6.5	Oligohaline	N.C.	N.C.	N.C.	89	11
18 (*Cyprideis* ostracod)	0.70851	2.45	7	Oligohaline	N.C.	N.C.	N.C.	88	12
24 (*Cyprideis* ostracod)	0.70814	1.57	4.5	Oligohaline	N.C.	N.C.	N.C.	91.5	8.5
27 (*Cyprideis* ostracod)	0.70806	1.57	4.5	Oligohaline	N.C.	N.C.	N.C.	92.5	7.5
34 (Charophyte)	0.70831	1.92	5.5	Oligohaline	N.C.	N.C.	N.C.	91	9
96 (*Cyprideis* ostracod)	0.70885	3.5	10	Oligohaline	N.C.	N.C.	N.C.	87	13
99 (*Neritina* gastropoda)	0.70802	1.4	4	Oligohaline	N.C.	N.C.	N.C.	93	7
12 (*Ammonia* foraminifera)	0.71051	N.C.	N.C.	N.C.	4.55	13	Oligohaline	74	26
13 (*Elphidium* foraminifera)	0.70909	N.C.	N.C.	N.C.	4.9	14	Oligohaline	83	17
16 (*Ammonia* foraminifera)	0.73424	N.C.	N.C.	N.C.	0.98	2.8	Oligohaline	5.5	94.5
19 (*Cyprideis* ostracod)	0.70889	N.C.	N.C.	N.C.	5.6	16	Mesohaline	86	14
21 (*Cyprideis* ostracod)	0.71021	N.C.	N.C.	N.C.	4.2	12	Oligohaline	75	25
25 (*Cyprideis* ostracod)	0.70978	N.C.	N.C.	N.C.	4.72	13.5	Oligohaline	79	21
33 (*Ammonia* foraminifera)	0.71026	N.C.	N.C.	N.C.	4.02	11.5	Oligohaline	75.5	24.5
36 (*Cyprideis* ostracod)	0.7092	N.C.	N.C.	N.C.	4.9	14	Oligohaline	84	16
Brazilian Eastern Amazonian basins									
2 (manatee vertebrae)	0.70872	N.C.	N.C.	N.C.	10.5	30	Mesohaline	N.C.	N.C.
3 (urchin)	0.70866	N.C.	N.C.	N.C.	9.8	28	Mesohaline	N.C.	N.C.
4 (crab claws)	0.7087	N.C.	N.C.	N.C.	10.15	29	Mesohaline	N.C.	N.C.
6 (*Myliobatis* ray teeth)	0.70885	N.C.	N.C.	N.C.	11.5	33	Mesohaline	N.C.	N.C.
N.C. = Not Calculated									

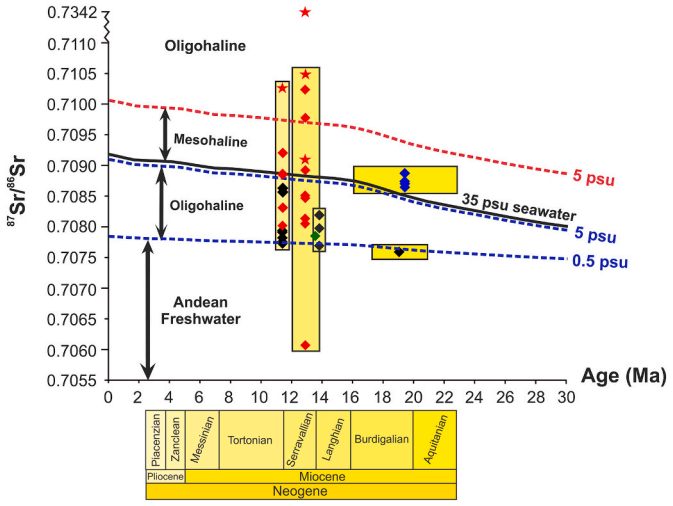


Fig. 6. Paleosalinity estimates for lower to lower upper Miocene fossil samples for Peruvian and Brazilian sites (foraminifera samples are marked as stars). Dashed blue (Andean water) and red (cratonic water) curves were calibrated based on the Miocene marine $^{87}Sr/^{86}Sr$ reference solid black curve (Howarth and McArthur, 1997) and the paleosalinity calculations respectively. (For interpretation of the references to colour in this figure legend, the reader is referred to the web version of this article.)

(0.70886) seawater. The models suggest that paleosalinity for these samples ranged between 0 and 3.5 psu, which corresponds to 0–7% of seawater content (Supplementary Datafile 1, Table 3). In details, samples 15, 18, 20, 24, 27, 34, 96 and 99 (*Cyprideis*, charophyte and *Neritina* gastropods) returned freshwater to oligohaline conditions (Fig. 6, Table 3).

ii. Seawater and cratonic rivers mixing models were applied to samples that yielded $^{87}Sr/^{86}Sr$ isotopic compositions above the $^{87}Sr/^{86}Sr$ ratios of Middle and Early Late Miocene seawater (0.70,876 and 0.70886 respectively). The models suggest that paleosalinity ranged between aproximately 1–5.6 psu, which corresponds to 2.8–16% of seawater content (Supplementary Datafile 1, Table 3). In details, samples 12, 13, 16, 19, 21, 25, 33 and 36 (*Cyprideis*, *Ammonia* or *Elphidum*) returned oligohaline to mesohaline conditions (Fig. 6, Table 3).

iii. Andean and cratonic rivers mixing model was applied using the $^{87}Sr/^{86}Sr$ isotopic composition of all the samples cited above and indicated a high Andean water contribution (range: 74–100%, Supplementary Datafile 1, Table 3) with exception of the sample 16 (*Ammonia*) that indicates dominant contribution of cratonic river waters (~94.5% cratonic, Supplementary Datafile 1, Table 3).

For the Early Miocene Eastern Amazonian samples (Pirabas Formation, Marajó Basin and Belém area), a binary mixture between seawater and cratonic rivers is the most probable scenario since the deposition of

Oligocene to Middle Miocene sediments had a cratonic provenance in this region (Figueiredo et al., 2009; Stewart et al., 2016; Van Soelen et al., 2017). Mixing models using $^{87}Sr/^{86}Sr$ isotopic composition of the analyzed Pirabas Formation samples suggest that paleosalinity range varies between approximately 9.8–11.5 psu, which corresponds to 28–33% of seawater content (Supplementary Datafile 1, Table 3). In details, samples 2, 3, 4 and 6 (crab claws, *Myliobatis* teeth, urchin and manatee vertebrae) returned mesohaline conditions (Fig. 6, Table 3).

5. Discussion

5.1. Influence of diagenesis and vital effect

Diagenesis may modify the original chemical and isotopic composition of carbonate rocks and fossils, leading to misinterpretation of paleoenvironmental conditions and paleosalinity estimations (Allan and Matthews, 1982). Since there is no evidence for hypogenic fluids in any of the rock unit studied, post-depositional isotopic modification of carbonate rocks and fossils could be related to interaction with clay-pore filling and organic matter accumulation. While organic matter would yield very negative $\delta^{13}C$ values, clay minerals could affect their primary Sr isotopic composition Jin et al., 2006 and references therein. To avoid diagenetic influence, we selected only well-preserved samples that have no visual signs of recrystallization or infilling material. Moreover, macrofossil specimens were cleaned with methanol and ultrasonic waves (Boyle, 1981; Rosenthal et al., 1999) to remove adherent clays onto their surfaces.

A potential diagenetic imprint may also be evaluated based on specific geochemical elemental concentrations such as Mn and Fe (Veizer, 1983; Jones et al., 1994; McArthur, 1994). Following Vonhof et al. (2003), we have used threshold values of 200 ppm for Fe and 100 ppm for Mn as threshold concentrations for indicating geochemical diagenetic imprint. All analyzed samples present Fe and Mn concentrations lower than the threshold concentrations (Table S2). This is an indication that diagenetic processes may not have affected significantly the primary isotopic composition of the fossils.

Biological control in skeletons formation (e.g., as metabolic processes) can lead to a broad intraspecific dispersion on the stable isotopic compositions of biomineralized tissues. These processes referred as 'vital effect' (Urey et al., 1951; Weiner and Dove, 2003) may control the isotopic composition of analyzed sample and thus prevent any paleoenvironmental interpretation based on isotopic composition. The vital effect on isotopic composition depends on the fossil groups and their ontogeny/growth rates parameters (McConnaughey, 1989; McConnaughey et al., 1997; Klein et al., 1996; Lorrain et al., 2004). For instance, $\delta^{13}C$ and $\delta^{18}O$ values of some mollusk and ostracod species may vary between 1 and 3‰ because of metabolic effects and/or calcification processes (e.g. Keatings et al., 2002; Ford et al., 2010; Pérez-Huerta and Andrus, 2010; Bournemann et al., 2012). Therefore, small fluctuations in $\delta^{13}C$ and $\delta^{18}O$ values in the isotopic composition of Early to Early Late Miocene ostracods and foraminifera samples in the same site (Fig. 3B and C) might be explained by 'vital effects'. However, we argue that the isotopic composition variation of a fossil taxon intra-site is narrower than the variation among-sites for the same taxon. This observation is supported by a statistical ANOVA test with $\delta^{13}C$ and $\delta^{18}O$ data of Early Late Miocene foraminifera (*Ammonia*) from sites CTA-44 and CTA-58 (Ucayali basin, Peru; Table S3), which are two distinct sites of the same age that have a high number of individual analyses. The ANOVA test returned *P*-values lower than 0.05 and hence, supported its null hypothesis: $\delta^{13}C$ and $\delta^{18}O$ variations among-sites are different statistically and are higher than intra-sites variations. Thus, we suggest that the isotopic variations among sites cannot be explained by 'vital effects' alone.

5.2. Fossils isotopic compositions and paleoenvironmental constraints

5.2.1. Eastern Amazonia (Early Miocene and recent)

Recent marine oysters from Atalaia Beach and foraminifera (*Amphistegina*) from the Equatorial Atlantic Ocean present $\delta^{13}C$ and $\delta^{18}O$ values characteristic to those of the Atlantic seawater (Fig. 4A). In addition, the foraminifera specimens yield a $^{87}Sr/^{86}Sr$ ratio (0.7091; Table S2) that is close to average global seawater range (0.709073–0.709243; e.g. Hodell et al., 1990; Brand et al., 2003; McArthur et al., 2006). Mangrove frog bones and crab claws from the Pará State present negative $\delta^{13}C$ and $\delta^{18}O$ signals that are close to the North American river's parameter. High $^{87}Sr/^{86}Sr$ isotopic ratios of these samples (0.71236 and 0.71209 respectively; Table S2) are consistent with a significant cratonic river contribution to the environment where those organisms lived.

In contrast, calcite-skeleton oyster from Mosqueiro Island has more negative $\delta^{13}C$ and $\delta^{18}O$ values, closer to those of aragonite-skeleton mollusks from Manaus (Fig. 4A). These lower isotopic values can be explained by the fact that the Mosqueiro Island holds a dense tropical forest and mangrove vegetation (rich in C3 plants) grown on podzols and hydromorphic soils. In addition, local surface water presents variable salinity (0–5 psu) and pH (5.4–7.19) values (Silva, 1975; Venturieri et al., 1998; Miranda et al., 2015; Rossetti, 2006). In such environment, local water's $\delta^{13}C$ (DIC and DOC) and $\delta^{18}O$ values are highly variable because of variations in precipitation/evaporation, freshwater/seawater influx, and input of soil-derived carbon driven by groundwater influx (Muylaert et al., 2005; Dalrymple and Choi, 2007). The $\delta^{13}C$ and $\delta^{18}O$ values of Early Miocene samples from Pirabas Formation (~ -0.5 to -3‰ and -1.5 to -5‰ respectively) are similar to those of San Francisco Bay estuary and close to those of Black Sea (Fig. 4C). As a matter of comparison, $\delta^{13}C$ and $\delta^{18}O$ values within a similar range (~ 2 to -4‰ and 1 to -5‰ respectively) are observed in transparent non-diagenetic microstructure of Early Miocene oysters from shallow-marine to estuarine deposits of the Mayo Formation at the Magallanes Basin, Argentinian Patagonia (Cuitiño et al., 2013). In addition, those samples exhibit $^{87}Sr/^{86}Sr$ ratios that plot within the mesohaline salinity field or close to the seawater line in Fig. 6. These suggest a significant marine influence into the Marajó Basin during the deposition of the Early Miocene Pirabas Formation. This interpretation agrees with the fossil content of the Pirabas Formation, which includes urchins, bryozoans, planktonic, ostracods, benthic foraminifera, and obligate marine vertebrates deposited in estuarine to shallow-marine paleoenvironments (Petri, 1957; Fernandes, 1984; Rossetti and Santos Jr., 2004; Ferreira, 2015; Martinez et al., 2017; Nogueira et al., 2019; Aguilera et al., 2020).

5.2.2. Western Amazonia (Early to Early Late Miocene and recent)

Sclerochronology isotopic data of recent mollusks from Peruvian and Brazilian Amazonia (Fig. 4A; Gaillard et al., 2019) show similar $\delta^{13}C$ but distinct $\delta^{18}O$ values. Brazilian bivalve shells (*Anodontites trapesialis*) present a large $\delta^{18}O$ variation (up to 7‰), similar to that provided by Kaandorp et al., (2003), and reflect an elevated isotopic variation of floodplain lakes influenced by the Solimões river seasonal dynamics. In contrast, Peruvian shells (*Anodontites elongatus*) present a lower $\delta^{18}O$ variation (4‰), indicating a habitat more influenced by the main river course water (Gaillard et al., 2019). Moreover, Peruvian shells tend to have more negative $\delta^{18}O$ values since Peruvian rivers receive ^{18}O-depleted waters from Andean mountain ranges (Ohlanders et al., 2013; Pfister et al., 2019). This is in agreement with lower $\delta^{18}O$ values of the river waters derived from the Andean region, such as the Solimões River, when compared to river waters derived from the Amazon floodplains or cratonic areas, such as those of the Negro River (Matsui et al., 1972; Rosário et al., 2016; Mulholland et al., 2015). Overall, the $\delta^{13}C$ and $\delta^{18}O$ values of analyzed fossil samples from Western Amazonia displays a distinct isotopic composition (approximately -6 to -17‰ and -2 to -10‰ respectively; Fig. 4B and C) when compared with Recent samples from the same region and from the Eastern Amazonia. These differences

in isotopic composition are statistically significant (Table S3).

Early to Middle Miocene fossil samples analyzed present isotopic compositions within or close to those of the North American rivers (Fig. 4C), including the ostracods and foraminifera from interpreted marine incursion and non-marine intervals of the 1-AS-33-AM well. Important variations of the $\delta^{18}O$ values of ostracods from this well (up to 5‰), are higher than the maximum natural variation observed for this taxon (3‰; Bournemann et al., 2012), indicating that changes in the evaporation rates or surface water influx may have affected their oxygen isotopic compositions (Bigg and Rohling, 2000). Hence, based on their stable isotopes compositions, we argue that those fossils probably lived in continental riverine environments, similar to ostracods, foraminifera (*Ammonia*) and mollusk's isotopic data from Peruvian (Porvenir) and Brazilian (Eurinepé and well 1AS-10-AM) sites studied by Gross et al., (2013, 2015) and Gross and Piller (2020). Paleosalinity estimate based on the $^{87}Sr/^{86}Sr$ isotopic composition of Early Miocene pacu teeth from Peruvian Contamana (CTA-63, Peru) also suggests a predominantly freshwater paleoenvironment (Table 3). Nonetheless, paleosalinity estimates based on the $^{87}Sr/^{86}Sr$ composition of Middle Miocene crab claws and pacu teeth from Peruvian sites (Contamana [CTA-45] and Tarapoto [TAR-31]) indicate predominantly oligohaline conditions to the paleoenvironments where these organisms lived (Table 3). Therefore, in the studied Peruvian sites, the Pebas Megawtland system might have been dominated by Andean freshwater in the Early Miocene (at

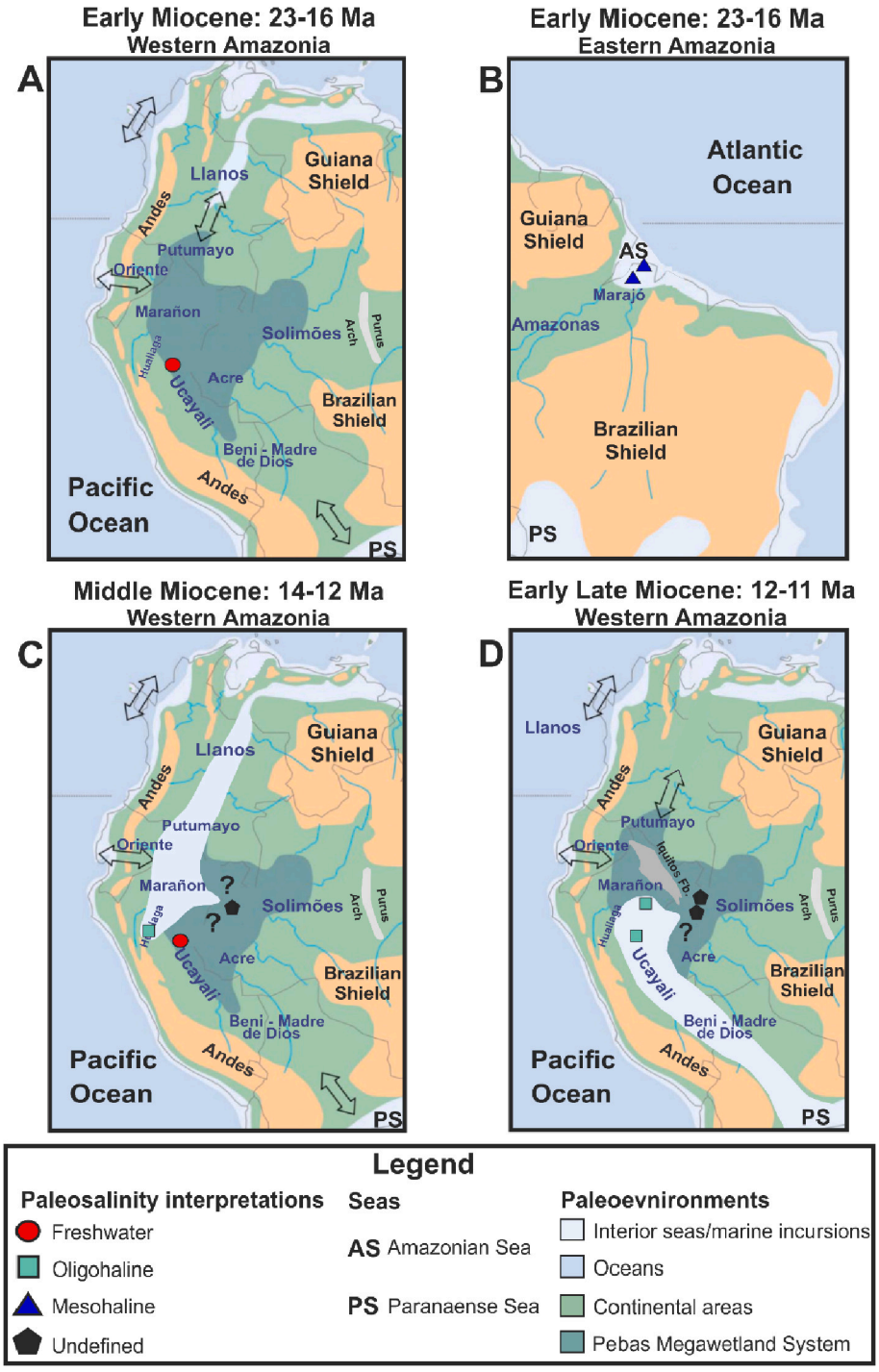


Fig. 7. Hypothetical maps of northern South America during early Miocene (A and B), middle Miocene (C) and early late Miocene (D) presenting the possible marine incursions interpreted according to the paleosalinity estimates of the samples analyzed for $^{87}Sr/^{86}Sr$ (Table 3). Sea entrances in Western Amazonia were interpreted based on Hermoza (2004), Ruiz et al. (2007), Antoine et al. (2016) and Jaramillo et al. (2017) works for north entrance, Nicolaidis and Coimbra (2008), Uba et al. (2009) and Louterbach et al. (2017) works for south entrance. Sea entrance in Eastern Amazonia was interpreted based on Santos et al. (2014), Távora et al. (2014) and Nogueira et al. (2019) works. Modified from Gross et al. (2015).

least in the time interval sampled), but it was affected by oligohaline waters, probably due to shallow-marine incursions in Middle Miocene times (Figs. 6 and 7A-B). Our results are comparable to the $^{87}Sr/^{86}Sr$ isotopic composition and paleosalinity estimates for Miocene mollusks from distinct Peruvian sites (Indiana, Pebas, Nuevo Horizonte, Porvenir and Santa Rosa) in Western Amazonia (Vonhof et al., 1998, 2003).

Although few samples also yield $\delta^{13}C$ and $\delta^{18}O$ values within the North American rivers parameter (e.g., CTA-43), most of the Early Late Miocene samples belonging to the Pebas Megawetland system present isotopic compositions plotting closer to the Great Lakes and the San Francisco estuary fields (Fig. 4B). Higher $\delta^{18}O$ may indicate lacustrine environmental conditions since lakes tend to present higher evaporation rates than rivers (Kaandorp et al., 2003; Wesselingh et al., 2006; Henderson and Shuman, 2010; Horton et al., 2016). In addition, some *Ammonia*, the only carbonate samples from CTA-44 locality, present very negative $\delta^{13}C$ values (Fig. 4B). A possible explanation for these values would be the influx of C3-derived compounds (Amazon C3 plants $\delta^{13}C$ signature range: −23‰ and − 34‰; Medina et al., 1999; Vogel et al., 1993; Diefendorf et al., 2010) by groundwater into surface water bodies (Klein et al., 1996; Gillikin et al., 2006; Samanta et al., 2015; Monger et al., 2015 and references therein). This hypothesis is supported by the CTA-44 outcrop lithology, which presents floodplain siltites and paleosols intercalated with conglomeratic channels rich in lignitous and/or pyritized floated wood (Antoine et al., 2016), organic material presumably the source of very negative $\delta^{13}C$ signals. Nevertheless, the stable isotopic compositions of the Early Late Miocene fossil samples analyzed here point to primarily continental paleonvironmental conditions, which conforms to the "Pantanal-like" hypothesis of Marivaux et al. (2020) for the Pebas Megawetland System. Paleosalinity estimates of samples 28, 37, 38, 40, 48, 49 and 94 (pacu and *Pristis* teeth, crab claws, *Cyprideis* and mollusks) from Peruvian Nuevo Horizonte and Contamana locaties (CTA-58, CTA-44 and CTA-43), however indicate the predominant presence of oligohaline waters (Table 3), suggesting that the Pebas Megawetland system in these sites may have been temporally subjected to oligohaline conditions during Early Late Miocene times (Figs. 6 and 7C). We argue that no definitive conclusion about paleosalinity estimates based on $^{87}Sr/^{86}Sr$ isotopic compositions can be drawn for Middle Miocene fossil samples from the Brazilian Amazonian sedimentary basins (1-AS-5-AM and 1-AS-7D-AM wells; Table 3). If a cratonic river vs seawater (samples 33 and 36) or Andean vs seawater (samples 34, 96 and 99) mixing models are considered, they might indicate a predominance of oligohaline water conditions in this area. However, freshwater conditions are also possible if Andean and cratonic water mixing is considered (Table 3).

Finally, our isotopic data suggest that the Pebas Megawetland system was predominantly a freshwater system alimented by both Andean and cratonic rivers and occasionally subjected to shallow-marine incursions, especially in Middle Miocene to Early Late Miocene times. To reconcile isotopic, sedimentological and paleontological evidences, we argue that the Miocene shallow-marine incursion intervals in Western Amazonia studied here were characterized by transitional paleoenvironments with a low contribution of seawater.

6. Conclusions

The C, O and $^{87}Sr/^{86}Sr$ isotopic compositions of the analyzed Miocene fossils from Eastern Amazonia (Marajó Basin, Brazil) and Western Amazonia (Ucayali and Huallaga Basins, Peru and the Solimões Basin, Brazil) yield the following conclusions:

- The isotopic compositions and paleosalinity estimates of fossils from the lower Miocene Pirabas Formation (Marajo Basin, Brazil) are characteristic of mesohaline to seawater conditions, reflecting the cyclical costal and shallow marine system characteristic of this unit.
- Early to Early Late Miocene fossils from Western Amazonia have more negative $\delta^{13}C$ and $\delta^{18}O$ signals (−17‰ to −6‰ for $\delta^{13}C$ and −10‰ to −2‰ for $\delta^{18}O$) than those of seawater, engulfed seas and estuaries parameters, suggesting a predominance of freshwater paleoenvironments in Western Amazonia during throughout the Miocene. Combination of organic matter decomposition and groundwater influxes likely to explain the low $\delta^{13}C$ values observed.
- Paleosalinity estimates based on the $^{87}Sr/^{86}Sr$ isotopic compositions of Peruvian fossil samples (Contamana, Tarapoto and Nuevo Horizonte sites) resulted in the following interpretations: i) freshwater conditions prevailed during Early Miocene; ii) oligohaline conditions (with seawater contribution below 10%) were observed intermittently in the Pebas Megawetland System during Middle and Early Late Miocene.
- Paleosalinity estimates of Brazilian Middle and Early Late Miocene samples from Western Amazonia Brazilian wells 1-AS-33-AM, 1-AS-5-AM and 1-AS-7D-AM are less constrained and could indicate: i) freshwater conditions if an Andean vs cratonic waters mixing model is considered or; ii) oligohaline to mesohaline conditions if cratonic vs seawater and Andean vs seawater models are considered.

Finally, our isotopic data suggest that the Pebas Megawetland system was dominantly a freshwater system in the was occasionally submitted to oligohaline influences probably resulted from shallow-marine incursions, as documented in Middle and Early Late Miocene times (Fig. 7). We suggest reconciling isotopic, sedimentological and paleontological evidences, which indicate the presence of transitional paleoenvironments associated to shallow-marine incursions in Western Amazonia throughout the Miocene. This is in perfect agreement with the palynological record and the mixture of terrestrial, obligate freshwater, and brackish-to-marine organisms recovered in a wide array of Miocene fossil assemblages in that vast domain.

Declaration of Competing Interest

The authors declare that they have no known competing financial interests or personal relationships that could have appeared to influence the work reported in this paper.

Acknowledgments

We thank an anonymous reviewer, Carlos Jaramillo and Hubert Vonhof, as well as the Editor Thomas J. Algeo for their valuable reviews and helpful comments that considerably improved this contribution. We are also grateful for the financial support given by the scientific institutions CAPES (Coordenação de Aperfeiçoamento de Pessoal de Nível Superior), COFECUB (Comité Français D'evaluation de la Coopération Universitaire et Scientifique avec le Brésil), CNPq (Conselho Nacional de Desenvolvimento Científico e Tecnológico) and IRD (Institut de Recherche pour le Développement). This study was supported by CAPES-COFECUB program Te 924/18 "Paléo-Amazone: evolution Néogène de l'Amazonie Brésilienne". In special, we want to thank Ana Paula Linhares (Museu Emilio Goeldi – Belém, Brazil) and Caio Gurgel Medeiros (CPRM – Rio de Janeiro, Brazil) for their assistance with the recovery and taxonomy of fossils from Amazonas State (Brazil) wells, Afonso César Rodrigues Nogueira (Universidade do Pará – Belém, Brazil) for his experienced guidance during fieldtrip at Pará State (Brazil) and Martino Giorgiani (Universidade de Brasília – Brasília, Brazil) for valuable discussions. Also, we thank Stéphane Brusset (Paul Sabatier University Toulouse III, Toulouse - France), Elton Dantas (Universidade de Brasília - Brasília, Brazil) and Lília Dias for their technical assistance in field trip to Acre State (Brazil) in 2018; and Ana Maria Ribeiro (Universidade Federal do Rio Grande do Sul – Porto Alegre, Brazil), Laurent Marivaux (ISEM – Montpellier, France) and Narla Stutz (UFRGS/ISEM) for their help in fieldwork, and the Military Police of the Acre State for its protection support during fieldtrip at Acre in 2019. Furthermore, we express our gratitude to the technicians Andre Gomes Pullen Parente, Jeane Grasyelle Silva Chaves and Luis Felipe

Baumotte Osorio from the Geochronology Laboratory of Universidade de Brasília for their efficiency in the analytical work.

Appendix A. Supplementary data

Supplementary material related to this article can be found online at Mendeley Data repository website at https://doi.org/10.17632/2smgvjr7np.4 or at https://doi.org/10.1016/j.palaeo.2021.110422.

References

Aguilera, O., de Araújo, O.M.O., Hendy, A., Nogueira, A.A., Nogueira, A.C., Maurity, C. W., da Silva-Caminha, S.A., 2020. Palaeontological framework from Pirabas Formation (North Brazil) used as potential model for equatorial carbonate platform. Mar. Micropaleontol. 154, 101813.

Allan, J.R., Matthews, R.K., 1982. Isotope signatures associated with early meteoric diagenesis. Sedimentology 29 (6), 797–817. https://doi.org/10.1111/j.1365-3091.1982.tb00085.x.

Allègre, C.J., Dupré, B., Négrel, P., Gaillardet, J., 1996. Sr-Nd-Pb isotope systematics in Amazon and Congo River systems: constraints about erosion processes. Chem. Geol. 131 (1–4), 93–112.

Antoine, P.-O., Baby, P., Benammi, M., Brusset, S., De Franceschi, D., Espurt, N., Goillot, C., Pujos, F., Salas-Gismondi, R., Tejada, J., Urbina, M., 2007. The Laventan Fitzcarrald local fauna, Amazonian Peru. In: 4th European Meeting on Paleontology and Stratigraphy of Latin America, 8. Cuadernos del Museo Geominero, Madrid, pp. 19–24.

Antoine, P.-O., Abello, M.A., Adnet, S., Altamirano Sierra, A.J., Baby, P., Billet, G., Boivin, M., Calderón, Y., Candela, A., Chabain, J., Corfu, F., Croft, D.A., Ganerød, M., Jaramillo, C., Klaus, S., Marivaux, L., Navarrete, R.E., Orliac, M.J., Parra, F., Pérez, M.E., Pujos, F., Rage, J.-C., Ravel, A., Robinet, C., Roddaz, M., Tejada-Lara, J. V., Vélez-Juarbe, J., Wesselingh, F.P., Salas-Gismondi, R., 2016. A 60-million-year Cenozoic history of western Amazonian ecosystems in Contamana, eastern Peru. Gondwana Res. 31, 30–59. https://doi.org/10.1016/j.gr.2015.11.001.

Barbosa Júnior, S.G., Teixeira, R.B.G., Cabral, M.C., Assano, M., Jomori, R.K., 2010. Tolerância de juvenis de Pacu *Piaractus mesopotamicus* à água salinizada. Nucleus Anim. 2 (2), 53–60.

Bayona, G., Jaramillo, C., Rueda, M., Reyes-Harker, A., 2007. Paleocene-Middle Miocene flexural-margin migration of the nonmarine Llanos foreland basin of Colombia. Ciencia, Tecnologia y Futuro 3, 141–160.

Bigg, G.R., Rohling, E.J., 2000. An oxygen isotope data set for marine waters proportion of SO in a sample of seawater is an excellent tracer of its past history $^{18}O/^{16}O$. J. Geophys. Res. 105, 8527–8535.

Blindow, I., 2000. Distribution of charophytes along the Swedish Coast in relation to salinity and eutrophication. Int. Rev. Hydrobiol. 85 (5–6), 707–717.

Boomer, I., Frenzel, P., Feike, M., 2016. Salinity-driven size variability in *Cyprideis torosa* (Ostracoda, Crustacea). J. Micropalaeontol. 36 (1), 63–69. https://doi.org/10.1144/jmpaleo2015-043.

Boonstra, M., Antoine, P.-O., Hoorn, C., Lammertsma, E.I., Ramos, M.I.F., 2015. Marine connections of Amazonia: evidence from foraminifera and dinoflagellate cysts (Early to middle Miocene, Colombia/Peru). Palaeogeogr. Palaeoclimatol. Palaeoecol. 417, 176–194. https://doi.org/10.1016/j.palaeo.2014.10.032.

Bouillon, S., Connolly, R.M., Gillikin, D.P., 2011. Use of Stable Isotopes to Understand Food Webs and Ecosystem Functioning in Estuaries, 7. Elsevier Inc, pp. 143–174. https://doi.org/10.1016/B978-0-12-374711-2.00711-7.

Bournemann, A., Pirkenseer, C.M., De Deckker, P., Speijer, R.P., 2012. Oxygen and carbon isotope fractionation of marine ostracod calcite from the eastern Mediterranean Sea. Chem. Geol. 310–311, 114–125. https://doi.org/10.1016/j.chemgeo.2012.03.028.

Boyle, E.A., 1981. Cadmium, zinc, copper, and barium in foraminifera tests. Earth Planet. Sci. Lett. 53, 11–35. https://doi.org/10.1016/0012-821X(81)90022-4.

Brand, U., Logan, A., Hiller, N., Richardson, J., 2003. Geochemistry of modern brachiopods: applications and implications for oceanography and paleoceanography. Chem. Geol. 198 (3–4), 305–334.

Bryant, J.D., Jones, D.S., Mueller, P.A., 1995. Influence of freshwater flux on 87Sr/86Sr chronostratigraphy in marginal marine environments and dating of vertebrate and invertebrate faunas. J. Paleontol. 69, 1–6.

Bryant, J.D., Jones, D.S., Mueller, P.A., Bryant, J.D., Jones, D.S., Mueller, P.A., 2015. Influence of Freshwater Flux on 87Sr / 86Sr in Chronostratigraphy Marginal Marine Environments and Dating of Vertebrate and Invertebrate Faunas. SEPM Society for Sedimentary Geology Paleontological Society.

Chabain, J., Antoine, P.-O., Altamirano-Sierra, A.J., Marivaux, L., Pujos, F., Salas-Gismondi, R., Adnet, S., 2017. Cenozoic batoid record from Contamana, Peru, with special focus on freshwater potamotrygonines (Chondrichthyes, Myliobatiformes) from the Pebas wetland system. Geobios 50, 389–400.

Chappell, J., Wang, P., 2001. Foraminifera as Holocene environmental indicators in the South Alligator River,Northern Australia. Quat. Int. 83-85, 47–62.

Coimbra, J.C., Carreño, A.L., Geraque, E.A., Eichler, B.B., 2007. Ostracodes (Crustacea) from Cananéia-Iguape estuarine/lagoon system and geographical distribution of the mixohaline assemblages in southern and southeastern Brazil. Iheringia. Sér. Zool. Porto Alegre 97 (3), 273–279.

Cousseau, M.B., De Figueroa, J.M., Díaz de Astarloa, E., Mabragaña, L.O., Lucifora, 2007. Rayas, chuchos y otros batoideos del Atlántico sudoccidental (34°-55°S). In: Mar del Plata. Argentina Instituto Nacional de Investigación y Desarrollo Pesquero, 102 pp.

Cuitiño, J., Santos, R., Scasso, R., 2013. Insights into the distribution of shallow-marine to estuarine Early miocene oysters from southwestern Patagonia: Sedimentologic and stable isotope constraints. Palaios 28, 583–598. https://doi.org/10.2110/palo.2012.p12-105r.

Dalrymple, J.W., Choi, K., 2007. Morphologic and facies trends through the fluvial–marine transition in tide-dominated depositional systems: a schematic framework for environmental and sequence-stratigraphic interpretation. Earth Sci. Rev. 81 (2007), 135–174.

Diefendorf, A.F., Mueller, K.E., Wing, S.L., Koch, P.L., Freeman, K.H., 2010. Global patterns in leaf ^{13}C discrimination and implications for studies of past and future climate. Proc. Natl. Acad. Sci. 107, 5738–5743.

Dueñas-Jimenez, H., 1980. Palynology of Oligocene–Miocene strata of borehole Q-E-22, Planeta Rica, Northern Colombia. Rev. Palaeobot. Palynol. 30, 313–328.

Dueñas-Jimenez, H., van der Hammen, T., 2007. Significado geologico y asociaciones palinologicas de las formaciones Diablo Inferior (Mioceno Tardio) y San Fernando Superior (Mioceno Medio). In: Piedemonte cuenca de los Llanos Orientales. Revista de la Academia Colombiana de Ciencias Exactas, Fisicas y Naturales, Colombia vol. 31, no. 121.

Espurt, N., Baby, P., Brusset, S., Roddaz, M., Hermoza, W., Regard, V., Antoine, P.-O., Salas-Gismondi, R., Bolaños, R., 2007. How does the Nazca Ridge subduction influence the modern Amazonian foreland basin? Geology 35, 515–518. https://doi.org/10.1130/G23237A.1.

Fernandes, J.M.G., 1984. Paleoecology of Formation Pirabas, Pará State. Anais da Academia Brasileira de Ciências 1, 330–340.

Ferreira, D.J.X., 2015. Inferências paleoambientais para o Nordeste da Amazônia Oriental a partir do estudo de registros fósseis e composição isotópica de carbono ($\delta^{13}C$) e oxigênio ($\delta^{18}O$) em rocha total de carbonatos da Formação Pirabas (PA). In: Mioceno Inferior. Universidade Federal do Pará, Belém, p. 120. Ph.D. Thesis.

Figueiredo, J., Hoorn, C., van der Ven, P., Soares, E., 2009. Late Miocene onset of the Amazon River and the Amazon deep-sea fan: evidence from the Foz do Amazonas Basin. Geology 37, 619–622. https://doi.org/10.1130/G25567A.1.

Firmino, K.C.S., 2009. Processos Osmorregulatórios no Caranguejo *Dilocarcinus pagei* (Decapoda, Trichodactylidae), Um Antigo Invasor da Água Doce: Estudo das Atividades (Na,K)-ATPase e V-ATPase Branquiais. Master dissertation. Faculdade de Filosofia, Ciências e Letras de Ribeirão Preto, Universidad de São Paulo, Ribeirão Preto. https://doi.org/10.11606/D.59.2009.tde-19082009-112806.

Ford, H.L., Schellenberg, S.A., Becker, B.J., Deutschman, D.L., Dyck, K.A., Koch, P.L., 2010. Evaluating the skeletal chemistry of Mytilus californianus as a temperature proxy: effects of microenvironment and ontogeny. Paleoceanography 25. PA 1203.

Fry, B., 2002. Conservative mixing of stable isotopes across estuarine salinity watershed gradients: a conceptual framework for monitoring influences on downstream fisheries production. Estuaries 25, 264–271.

Gaillard, B., Lazareth, C.E., Lestrelin, H., Dufour, E., Santos, R.V., Freitas, C.E.C., Pouilly, M., 2019. Seasonal oxygen isotope variations in freshwater bivalve shells as recorders of Amazonian rivers hydrogeochemistry. Isot. Environ. Health Stud. 1–15. https://doi.org/10.1080/10256016.2019.1666120.

Gillikin, D.P., Lorrain, A., Bouillon, S., Dehairs, F., Willenz, P., 2006. $\delta^{13}C$ in *Mytilus edulis* shells : relation to salinity, DIC, phytoplankton and metabolism. Org. Geochem. 37, 1371–1382.

Gingras, M.K., Räsänen, M.E., Pemberton, S.G., Romero, L.P., 2002a. Ichnology and sedimentology reveal depositional characteristics of bay margin parasequences in the Miocene Amazonian foreland basin. J. Sediment. Res. 72, 871–883.

Gingras, M.K., Räsänen, M.E., Ranzi, A., 2002b. The signifi cance of bioturbated inclined heterolithic stratification in the southern part of the Miocene Solimões Formation, Rio Acre: Amazonia Brazil. Palaios 17, 591–601.

Góes, A.M., Rossetti, D.F., Nogueira, A.C.R., 1990. Toledo, P.M. 1990. Modelo deposicional preliminar da Formação Pirabas no nordeste do Estado do Pará. Boletim do Museu Paraense Emílio Goeldi. Série Ciências da Terra 2, 3–15.

Gómez, E., Jordan, T.E., Allmendinger, R.W., Cardozo, N., 2005. Development of the Colombian forelandbasin system as a consequence of diachronous exhumation of the northern Andes. Geol. Soc. Am. Bull. 117 (9–10), 1272–1292. https://doi.org/10.1130/B25456.1.

Gross, M., Piller, W., 2020. Saline waters in Miocene Western Amazonia – an alternative view. Front. Earth Sci. 8 https://doi.org/10.3389/feart.2020.00116 article 116.

Gross, M., Piller, W., Ramos, M.I.F., Paz, J., 2011. Late Miocene sedimentary environments in south-western Amazonia (Solimões Formation; Brazil). J. S. Am. Earth Sci. 32, 169–181. https://doi.org/10.1016/j.jsames.2011.05.004.

Gross, M., Ramos, M.I.F., Caporaletti, M., Piller, W., 2013. Ostracods (Crustacea) and their palaeoenvironmental implication for the Solimões Formation (Late Miocene; Western Amazonia/Brazil). J. S. Am. Earth Sci. 42, 216–241. https://doi.org/10.1016/j.jsames.2012.10.002.

Gross, M., Ramos, M.I.F., Piller, W., 2014. On the Miocene *Cyprideis* species flock (Ostracoda; Crustacea) of Western Amazonia (Solimões Formation): refining taxonomy on species level. Zootaxa 3899, 001–069. https://doi.org/10.11646/zootaxa.3899.1.1.

Gross, M., Ramos, M.I.F., Piller, W.E., 2015. A minute ostracod (Crustacea: Cytheromatidae) from the Miocene Solimões Formation (western Amazonia, Brazil): evidence for marine incursions? J. Syst. Palaeontol. 14 (7), 581–602. https://doi.org/10.1080/14772019.2015.1078850.

Henderson, A.K., Shuman, B.N., 2010. Differing controls on river- and lake-water hydrogen and oxygen isotopic values in the western United States. Hydrol. Process. 24, 3894–3906. https://doi.org/10.1002/hyp.7824.

Hermoza, W., 2004. Dynamique Tectono-Sédimentaire et Restauration Séquentielle du Rétro-Bassin D'avant-Pays des Andes Centrals. PhD thesis. Université de Paul Sabatier de Toulouse III, 296 pp.

Hermoza, W., Brusset, S., Baby, P., Gil, W., Roddaz, M., Guerrero, N., Bolañoz, M., 2005. The Huallaga foreland basin evolution: thrust propagation in a deltaic environment, northern Peruvian Andes. J. S. Am. Earth Sci. 19, 21–24.
Hodell, D.A., Mead, G.A., Mueller, P.A., 1990. Variation in the strontium isotopic composition of Seawater (8 Ma to Present): implications for chemical weathering rates and dissolved fluxes to the Oceans. Chem. Geol. 80 (4), 291–307.
Hodell, D.A., Kamenov, G.D., Hathorne, E.C., Zachos, J.C., Röhl, U., Westerhold, T., 2007. Variations in the strontium isotope composition of seawater during the Paleocene and Early Eocene from ODP Leg 208 (Walvis Ridge). Geochem. Geophys. Geosyst. 8, Q09001 https://doi.org/10.1029/2007GC001607.
Hohenegger, J., Piller, W.E., Baal, C., 1993. Horizontal and vertical spatial microdistribution of foraminifers in the shallow subtidal Gulf of Trieste, Northem Adriatic Sea. J. Foraminifer. Res. 23 (2), 79–101.
Holmden, C., Muehlenbachs, K., Creaser, R.A., 1997. Depositional environment of the Early Cretaceous ostracode zone: Paleohydrologic constraints from O, C, and Sr isotopes. In: Pemberton, S.G., James, D.P. (Eds.), Petroleum geology of the Cretaceous Manville Group, 18. Canadian Society of Petroleum Geologists Memoir, Western Canada, pp. 77–92.
Hoorn, C., 1990. Evolución de los ambientes sedimentarios durante el terciario y el Cuaternario en la Amazonia Colombiana. Colomb. Amazon 4 (2), 97–126.
Hoorn, C., 1993. Marine incursions and the influence of Andean tectonics on the Miocene depositional history of northwestern Amazonia: results of a palynostratigraphic study. Palaeogeogr. Palaeoclimatol. Palaeoecol. 105, 267–309.
Hoorn, C., 1994. An environmental reconstruction of the palaeo-Amazon River system (Middle-Late Miocene, NW Amazonia). Palaeogeogr. Palaeoclimatol. Palaeoecol. 112, 187–238. https://doi.org/10.1016/0031-0182(94)90074-4.
Hoorn, C., Wesselingh, F., 2010. Amazonia, Landscape and Species Evolution: A Look into the Past. John Wiley & Sons, Hoboken. https://doi.org/10.1002/9781444306408.
Hoorn, C., Guerrero, J., Sarmiento, G., Lorente, M., 1995. Andean tectonics as a cause for changing drainage patterns in Miocene northern South America. Geology 23, 237–240.
Hoorn, C., Wesselingh, F., ter Steege, H., Bermudez, M., Mora, A., Sevink, J., Sanmartin, I., Meseguer, A.S., Anderson, C.L., Figueiredo, J., Jaramillo, C., Riff, D., Negri, F., Hooghiemstra, H., Lundberg, J., Stadler, T., Särkinen, T., Antonelli, A., 2010. Amazonia through time: Andean uplift, climate change, landscape evolution, and biodiversity. Science (New York, N.Y.) 330, 927–931. https://doi.org/10.1126/science.1194585.
Horbe, A.M.C., Roddaz, M., Gomes, L.B., Castro, R.T., Dantas, E.L., do Carmo, D. A., 2019. Provenance of the Neogene sediments from the Solimões Formation (Solimões and Acre Basins), Brazil. J. S. Am. Earth Sci. https://doi.org/10.1016/j.jsames.2019.05.004.
Horton, T.W., Defliese, W.F., Tripati, A.K., Oze, C., 2016. Evaporation induced 18O and 13C enrichment in lake systems: a global perspective on hydrologic balance effects. Quat. Sci. Rev. 131, 365–379. https://doi.org/10.1016/j.quascirev.2015.06.030.
Hovikoski, J., Gingras, M., Räsänen, M., Rebata, L., Guerrero, J., Ranzi, A., et al., 2007a. The nature of Miocene Amazonian epicontinental embayment: High-frequency shifts of the low-gradient coastline. GSA Bull. 119, 1506–1520.
Hovikoski, J., Räsänen, M., Gingras, M., Lopez, S., Ranzi, A., Melo, J., 2007b. Palaeogeographical implications of the Miocene Quendeque Formation (Bolivia) and tidally-influenced strata in the southwestern Amazonia. Palaeogeogr. Palaeocl. 243, 23–41.
Hovikoski, J., Wesselingh, F.P., Räsänen, M., Gingras, M., Vonhof, H.B., 2010. Marine influence in Amazonia: Evidence from the geological record. In: Hoorn, C., Wesseling, F.P. (Eds.), Amazonia: Landscape and Species Evolution, a Look into the Past. Wiley-Blackwell, Oxford, pp. 143–161.
Howarth, R.J., McArthur, J.M., 1997. Statistics for strontium isotope stratigraphy: a robust LOWESS fit to the marine Sr-isotope curve for 0–206 Ma, with look-up table for derivation of numeric age. J. Geol. 105, 441–456.
Hurtado, C., Roddaz, M., Santos, R.V., Baby, P., Antoine, P.-O., Dantas, E.L., 2018. Cretaceous-Early Paleocene drainage shift of Amazonian rivers driven by Equatorial Atlantic Ocean opening and Andean uplift as deduced from the provenance of northern Peruvian sedimentary rocks (Huallaga basin). Gondwana Res. 63, 152–168. https://doi.org/10.1016/j.gr.2018.05.012.
Ingram, B.L., DePaolo, D.J., 1993. A 4,300-year strontium isotope record of estuarine paleosalinity in San Francisco Bay, California. Earth Planet. Sci. Lett. 119, 103–119.
Ingram, B.L., Conrad, M.E., Ingle, J.C., 1996. Stable isotope and salinity systematics in estuarine waters and carbonates: San Francisco Bay. Geochim. Cosmochim. Acta 60, 455–467. https://doi.org/10.1016/00167037(95)00398-3.
Jaramillo, C., Rueda, M., Torres, V., 2011. A palynological zonation for the Cenozoic of the Llanos and Llanos Foothills of Colombia. Palynology 35, 46–84. https://doi.org/10.1080/01916122.2010.515069.
Jaramillo, C., Romero, I., D'Apolito, C., Bayona, G., Duarte, E., Louwye, S., Escobar, J., Luque, J., Carrillo-Briceño, J.D., Zapata, V., Mora, A., Schouten, S., Zavada, M., Harrington, G., Ortiz, J., Wesselingh, F.P., 2017. Miocene flooding events of western Amazonia. Sci. Adv. 3. https://doi.org/10.1126/sciadv.1601693.
Jin, Z.D., Cao, J., Wu, J., Wang, S., 2006. A Rb/Sr record of catchment weathering response to Holocene climate change in Inner Mongolia. Earth Surf. Process. Landf. 31, 285–291. https://doi.org/10.1002/esp.1243.
Jones, C.E., Jenkyns, H.C., Coe, A.L., Hesselbo, S.P., 1994. Strontium isotopic variations in Jurassic and cretaceous seawater. Geochim. Cosmochim. Acta 58, 3061–3074.
Kaandorp, R.J.G., Vonhof, H.B., del Busto, C., Wesselingh, F., Ganssen, G.M., Marmol, A. E., 2003. Seasonal stable isotope variations of the modern Amazonian freshwater bivalve Anodontites trapesialis. Palaeogeogr. Palaeocl. 194, 339–354.
Keatings, K.W., Heaton, T.H.E., Holmes, J.A., 2002. Carbon and oxygen isotope fractionation in non-marine ostracods: results from a 'natural culture' environment. Geochim. Cosmochim. Acta 66, 1701–1711.
Keith, M., Anderson, G., Eichler, R., 1964. Carbon and oxygen isotope composition of mollusk shells from marine and freshwater environments. Geochim. Cosmochim. Acta 28, 1757–1786.
Kern, A., Gross, M., Galeazzi, C., Pupim, F., Sawakuchi, A., Almeida, R., Piller, W., Kuhlmann, G., Basei, M., 2020. Re-investigating Miocene age control and paleoenvironmental reconstructions in western Amazonia (northwestern Solimões Basin, Brazil). Palaeogeogr. Palaeoclimatol. Palaeoecol. 109652 https://doi.org/10.1016/j.palaeo.2020.109652.
Klaus, S., Magalhães, C., Salas-Gismondi, R., Gross, M., Antoine, P.O., 2017. Palaeogene and Neogene brachyurans of the Amazon basin: a revised first appearance date for primary freshwater crabs (Brachyura, Trichodactylidae). Crustaceana 90, 953–967. https://doi.org/10.1163/15685403-00003629.
Klein, R.T., Lohmann, K.C., Thayer, C.W., January, R., 1996. Sr/Ca and $^{13}C/^{12}C$ ratios in skeletal calcite of MytiZus trossulus : covariation with metabolic rate, salinity, and carbon isotopic composition of seawater. Geochim. et Cosmochim. Act. 60, 4207–4221.
Latrubesse, E., da Silva, S., Cozzuol, M., Absy, M., 2007. Late Miocene continental sedimentation in southwestern Amazonia and its regional signifi cance: Biotic and geological evidence. J. S. Am. Earth Sci. 23, 61–80.
Latrubesse, E., Cozzuol, M., Silva Caminha, S., Rigsby, C., Absy, M., Jaramillo, C., 2010. The Late Miocene Paleogeography of the Amazon Basin and the evolution of the Amazon River system. Earth Sci. Rev. 99, 99–124. https://doi.org/10.1016/j.earscirev.2010.02.005.
Linhares, A.P., Ramos, M.I.F., Gross, M., Piller, W.E., 2011. Evidence for marine influx during the Miocene in southwestern Amazonia, Brazil. Geol. Colomb. 36, 91–104.
Linhares, A.P., de Gaia, V. do C.S., Ramos, M.I., 2017. The significance of marine microfossils for paleoenvironmental reconstruction of the Solimões Formation (Miocene), western Amazonia, Brazil. J. S. Am. Earth Sci. 79, 57–66. https://doi.org/10.1016/j.jsames.2017.07.007.
Linhares, A.P., Ramos, M.I.F., Gaia, V., Friaes, Y., 2019. Integrated biozonation based on palynology and ostracods from the Neogene of Solimões Basin, Brazil. J. S. Am. Earth Sci. 91 https://doi.org/10.1016/j.jsames.2019.01.015.
Logvina, E., Mazurenko, L., Prasolov, E., 2004. Isotopic composition of carbon-13 and oxygen-18 from authigenic carbonates. In: Black Sea Region. AGU Spring Meeting Abstracts.
Lorrain, A., Paulet, Y.M., Chauvaud, L., Dunbar, R.B., Mucciarone, D., Fontugne, M., 2004. ^{13}C variation in scallop shells: increasing metabolic carbon contribution with body size? Geochim. Cosmochim. Acta 68, 3509–3519.
Louterbach, M., Martin, R., Antoine, P.-O., Marivaux, L., Adnet, S., Bailleul, J., Dantas, E., Santos, R.V., Chemale Jr., F., Baby, P., Sanchez, C., Calderon, Y., 2017. Provenance record of late Maastrichtian, late Paleocene Andean Mountain building in the Amazonian retroarc foreland basin (Madre de Dios basin Peru). Terra Nova 30 (1), 17–23. https://doi.org/10.1111/ter.12303.
Magalhães, C., 1999. In: Buckup, L., Bond-Buckup, G., Os Crustáceos do Rio Grande do Sul (Eds.), Família Trichodactylidae (caranguejos braquiúros da água doce). da Universidade Federal do Rio Grande do Sul, pp. 486–490, 514 p.
Marivaux, L., Aguirre-Dias, W., Benites-Palomino, A., Billet, G., Boivin, M., Pujos, F., Salas-Gismondi, R., Tejada-Lara, J.V., Varas-Malca, R.M., Antoine, P.-O., 2020. New record of *Neosaimiri* (Cebidae, Platyrrhini) from the late Middle Miocene of Peruvian Amazonia. J. Hum. Evol. 146, 102835. https://10.1016/j.jhevol.2020.102835.
Martinez, S., Ramos, M.I.F., McArthur, J.M., Del Río, C.J., Thirlwall, M.F., 2017. Late Burdigalian (Miocene) age for pectinids (Mollusca-Bivalvia) from the Pirabas Formation (northern Brazil) derived from Sr-isotope ($^{87}Sr/^{86}Sr$) data. N. Jb. Geol. Paläont. Abh. 284 (1), 57–64.
Mathalone, J.M.P., Montoya, R.M., 1995. Petroleum geology of the sub-Andean basins of Peru. In: Tankard, A.J., Suárez, R.S., Welsink, H.J. (Eds.), Petroleum Basins of South America, 62. AAPG Memoir, pp. 423–444.
Matsui, E., Salati, E., Brinkmann, W.L.F., Friedman, I., 1972. Vazões relativas dos rios Negro e Solimões através das concentrações de 18O. Acta Amazon. 3 (2), 31–46.
McArthur, J.M., 1994. Recent trends in strontium isotope stratigraphy. Terra Nova 6, 331–358.
McArthur, J.M., Rio, D., Massari, F., et al., 2006. A revised Pliocene Record for Marine87Sr/86Sr used to date an interglacial event recorded in the cockburn Island formation, Antarctic Peninsula. Palaeogeogr. Palaeoclimatol. Palaeoecol. 242 (1/2), 126–136.
McConnaughey, T.A., 1989. ^{13}C and ^{18}O isotopic disequilibria in biological carbonates: I. Patterns. Geochim. Cosmochim. Acta 53, 151–162.
McConnaughey, T.A., Burdett, J., Whelan, J.F., Paull, C.K., 1997. Carbon isotopes in biological carbonates: respiration and photosynthesis. Geochim. Cosmochim. Acta 61, 611–622.
McEachran, J.D., Aschliman, N., 2004. Phylogeny of Batoidea. In: Carrier, J.C., Musick, J.A., Heithaus, M.R. (Eds.), Biology of Sharks and their Relatives. CRC Press, Boca Raton, FL, pp. 79–113.
Medeiros, C.G., Do Carmo, D.A., Antonietto, L.S., Boush, L.E.P., 2019. The Ostracods from Solimões Formation, Brazil: An Alternative Biostratigraphic Zonation for the Neogene of Amazonia (Revista Brasileira de Paleontologia).
Medina, E., Martinelli, L.A., Barbosa, E., Victoria, R.L., 1999. Natural abundance of ^{13}C in tropical grasses from the INPA, Instituto Nacional de Pesquisas da Amazônia, herbarium. Br. J. Bot. 22 (1), 44–51. https://doi.org/10.1590/S0100-84041999000100007.
Meyer, J., Wrozyna, C., Gross, M., et al., 2017. Morphological and geochemical variations of *Cyprideis* (Ostracoda) from modern waters of the northern Neotropics. Limnology 18, 251–273. https://doi.org/10.1007/s10201-016-0504-9.

Miranda, M., Santos, M., Pereira, J.A., Mesquita, K., 2015. Índices de qualidade da água da Ilha de Mosqueiro-PA. Revista DAE 64, 74–81. https://doi.org/10.4322/dae.2015.005.

Monger, H.C., Kraimer, R.A., Khresat, S., Cole, D.R., Wang, X., Wang, J., 2015. Sequestration of inorganic carbon in soil and groundwater. Geology 43 (5), 375–378. https://doi.org/10.1130/G36449.1.

Monsch, K.A., 1998. Miocene fish faunas from the northwestern Amazonia basin (Colombia, Peru, Brazil) with evidence of marine incursions. Palaeogeogr. Palaeoclimatol. Palaeoecol. 143, 31–50.

Mook, W.G., Vogel, J.C., 1968. Isotopic equilibrium between shells and their environment. Science 159, 874–875.

Mulholland, D., Poitrasson, F., Boaventura, G., Allard, T., Vieira, L., Santos, R., Mancini, L., Seyler, P., 2015. Insights into iron sources and pathways in the Amazon River provided by isotopic and spectroscopic studies. Geochim. Cosmochim. Acta 150. https://doi.org/10.1016/j.gca.2014.12.004.

Murray, J.W., 1991. Ecology and Paleoecology of Benthic Foraminifera. Longman, Harlow.

Murray, J.W., 2006. Ecology and Applications of Benthic Foraminifera. Cambridge University Press, Cambridge.

Muylaert, K., Dasseville, R., De Brabandere, L.D., Dehairs, F., Vyverman, W., 2005. Dissolved organic carbon in the freshwater tidal reaches of the Schelde estuary. Estuar. Coast. Shelf Sci. 64, 591–600.

Nicolaidis, D., Coimbra, J., 2008. *Perissocytheridea carrenoae* sp nov (Crustacea, Ostracoda) and associated calcareous microfauna from Yecua Formation (Miocene), Bolivia. Rev. Brasil. de Paleontol. 11, 179–186. https://doi.org/10.4072/rbp.2008.3.04.

Nogueira, A., Ramos, M.I.F., Hunt, G., 2019. Taxonomy of ostracods from the Pirabas Formation (Upper Oligocene to Lower Miocene), Eastern Amazonia (Pará State, Brazil). Zootaxa 4573. https://doi.org/10.11646/zootaxa.4573.1.1.

Nuttall, C., 1990. A review of the Tertiary nonmarine molluscan faunas of the Pebasian and other inland basins of north-western South America. Bull. Br. Museum (Natural History) Geol. 45, 165–372.

Ohlanders, N., Rodriguez, M., McPhee, J., 2013. Stable water isotope variation in a Central Andean watershed dominated by glacier and snowmelt. Hydrol. Earth Syst. Sci. 17 (3), 1035–1050. https://doi.org/10.5194/hess-17-1035-2013.

Palmer, M.R., Edmond, J.M., 1992. Controls over the strontium isotope composition of river water. Geochim. Cosmochim. Acta 56, 2099–2111.

Parra, M., Mora, A., Jaramillo, C., Strecker, M., Sobel, E., Quiroz, L., Rueda, M., Torres, V., 2009. Orogenic wedge advance in the northern Andes: Evidence from the Oligocene-Miocene sedimentary record of the Medina Basin, Eastern Cordillera, Colombia. Geol. Soc. Am. Bull. - GEOL SOC AMER BULL. 121, 780–800. https://doi.org/10.1130/B26257.1.

Pérez-Huerta, A., Andrus, C.F.T., 2010. Vital effects in the context of biomineralization. Seminarios SEM 7, 35–45.

Petri, S., 1957. Foraminíferos Miocênicos da formação Pirabas. Boletim Da Faculdade De Filosofia Ciências E Letras, 16. Universidade De São Paulo, Geologia, pp. 1–80. https://doi.org/10.11606/issn.2526-3862.bffcluspgeologia.1957.121843.

Pfister, L., Grave, C., Beisel, J.N., McDonnell, J.J., 2019. A global assessment of freshwater mollusk shell oxygen isotope signatures and their relation to precipitation and stream water. Sci. Rep. 9, 4312. https://doi.org/10.1038/s41598-019-40369-0.

Räsänen, M.E., Linna, A.M., Santos, J.C.R., Negri, F.R., 1995. Late miocene tidal deposits in the Amazonian foreland basin. Science 269, 386–390. https://doi.org/10.1126/science.269.5222.386.

Rebata, L.A., 2012. Peru. Doctoral thesis. The Sedimentology, Ichnology and Hydrogeochemistry of the Late Miocene, Marginal Marine, Upper Pebas and Nauta Formations, Amazonian Foreland Basin, vol. 275. University of Turku, Annales Universitatis Turkuensis, pp. 1–45. ISBN 978-951-29-5217-5.

Rebata, L., Gingras, M., Räsänen, M., Barberi, M., 2006. Tidal-channel deposits on a delta plain from the Upper Miocene Nauta formation, Marañon Foreland Sub-basin, Peru. Sedimentology 53, 971–1013.

Roddaz, M., Viers, J., Brusset, S., Baby, P., Hérail, G., 2005. Sediment provenances and drainage evolution of the Neogene Amazonian foreland basin. Earth Planet. Sci. Lett. 239, 57–78. https://doi.org/10.1016/j.epsl.2005.08.007.

Roddaz, M., Brusset, S., Baby, P., Hérail, G., 2006. Miocene tidal influenced sedimentation to continental Pliocene sedimentation in the forebulge-backbulge depozones of the Beni-Mamore foreland basin (northern Bolivia). J. S. Am. Earth Sci. 20, 79–96.

Roddaz, M., Hermoza, W., Mora, A., Baby, P., Pa, M., Christophoul, F., Brusset, S., Espurt, N., 2010. Cenozoic sedimentary evolution of the Amazonian foreland basin system. In: Hoorn, C., Wesselingh, F. (Eds.), 2010. Amazonia, Landscape and Species Evolution: A Look into the Past, ch.5, pp. 61–88.

Rosário, R.B., Borba, T.A.C., Santos, A.S., Rollnic, M., 2016. Variability of salinity in Pará River Estuary: 2D analysis with flexible mesh model. J. Coast. Res. S1 (75), 128–132.

Rosenthal, Y., Field, M.P., Sherrell, R.M., 1999. Precise determination of element/calcium ratios in calcareous samples using sector field inductively coupled plasma mass spectrometry. Anal. Chem. 71, 3248–3253. https://doi.org/10.1021/ac981410x.

Rossetti, D., 2006. Evolução sedimentar miocênica nos estados do Pará e Maranhão. Geologia USP. Série Científica 6 (2), 7–18. https://doi.org/10.5327/S1519-874X2006000300003.

Rossetti, D.F., Santos Jr., A.E.A., 2004. Facies architecture in a tectonically-influenced estuarine incised valley fill of Miocene age, Northern Brazil. J. S. Am. Earth Sci. 17, 267–284.

RStudio Team, 2020. RStudio: Integrated Development for R. RStudio, PBC, Boston, MA. URL. http://www.rstudio.com/.

Ruiz, G.M.H., Seward, D., Winkler, W., 2007. Evolution of the Amazon Basin in Ecuador with special reference to hinterland tectonics: data from zircon fission-track and heavy mineral analysis. Dev. Sedimentol. 58, 907–934.

Rull, V., 2001. A quantitative palynological record from the Early Miocene of western Venezuela, with emphasis on mangroves. Palynology 25 (1), 109–126.

Salas-Gismondi, R., Baby, P., Antoine, P.-O., Pujos, F., Benammi, M., Espurt, N., Brusset, S., Urbina, M., De Franceschi, D., 2006. Late middle Miocene vertebrates from the Peruvian Amazonian basin (Inuya and Mapuya Rivers, Ucayali). In: Fitzcarrald Expedition 2005. XIII Congreso Peruano de Geología, pp. 643–646.

Salas-Gismondi, R., Antoine, P.-O., Baby, P., Benammi, M., Espurt, N., Pujos, F., Tejada, J., Urbina, M., De Franceschi, D., 2007. Middle Miocene crocodiles from the Peruvian Amazonian basin (Fitzcarrald Arch). 4th European Meeting on Paleontology and Stratigraphy of Latin America. Cuadernos del Museo Geominero 8, 355–360.

Salas-Gismondi, R., Flynn, J.J., Baby, P., Tejada-Lara, J., Wesselingh, F.P., Antoine, P.-O., 2015. A Miocene hyperdiverse crocodylian community reveals peculiar trophic dynamics in proto-Amazonian mega-wetlands. Proc. R. Soc. B. https://doi.org/10.1098/rspb.2014.2490.

Samanta, S., Dalai, T.K., Pattanaik, J.K., Rai, S.K., Mazumdar, A., 2015. Dissolved inorganic carbon (DIC) and its $d^{13}C$ in the Ganga (Hooghly) River estuary, India: evidence of DIC generation via organic carbon degradation and carbonate dissolution. Geochim. Cosmochim. Acta 165, 226–248.

Sanjuan, J., Martín-Closas, C., 2012. Charophyte palaeoecology in the Upper Eocene of the Eastern Ebro basin (Catalonia, Spain). Biostratigraphic implications. Palaeogeogr. Palaeoclimatol. Palaeoecol. 365–366, 247–262.

Santos, R.V., Sondag, F., Cochonneau, G., Lagne, C., Bunet, P., Hattingh, K., Chaves, J.G. S., 2014. Seasonal $^{87}Sr/^{86}Sr$ variations in rivers of the Amazon basin. Hydrol. Process. 29 (2), 187–197.

Schmitz, B., Werdelin, L., Forey, P., Bendix-Almgreen, S.E., 1991. $^{87}Sr/^{86}Sr$, Na, F, Sr, and La in skeletal fish debris as a measure of the paleosalinity of fossil-fish habitats. Geol. Soc. Am. Bull. 103, 786–794.

Silva, B.N.R., 1975. Levantamento de reconhecimento detalhado dos solos da ilha do mosqueiro –PA com auxílio de fotointerpretação. Piracicaba. In: Escola Superior de Agricultura Luiz de Queiroz, 156 p. (Dissertação de Mestrado).

Souza-Bastos, L.R., Bastos, L.P., Carneiro, P.C.F., Freire, C.A., 2016. Acute salt exposure of the freshwater Characiformes: Pacu (*Piaractus mesopotamicus*, Holmberg 1887), Tambaqui (*Colossoma macropomum*, Cuvier 1818), and their hybrid "Tambacu.". Aquaculture 465, 352–358. https://doi.org/10.1016/j.aquaculture.2016.09.028.

Spencer, J.E., Patchett, P.J., 1997. Sr isotope evidence for a lacustrine origin for the upper Miocene to Pliocene Bouse Formation, lower Colorado River trough, and implications for timing of Colorado Plateau uplift. Geol. Soc. Am. Bull. 109, 767–778.

Stevens, J.D., McAuley, R.B., Simpfendorfer, C.A., Pillans, R.D., 2008. Spatial distribution and habitat utilisation of sawfish (*Pristis* spp) in relation to fishing in northern Australia. In: A Report to Department of the Environment, Water, Heritage and the Arts.

Stewart, J.A., Gutjahr, M., James, R.H., Anand, P., Wilson, P.A., 2016. Influence of the Amazon River on the Nd isotope composition of deep water in the western equatorial Atlantic during the Oligocene–Miocene transition. Earth Planet. Sci. Lett. 454, 132–141. https://doi.org/10.1016/j.epsl.2016.08.037.

Távora, V.A., de Souza, B.L.P., Neto, I.L.A.N., 2014. Micropaleontology of the Reef Facies of the Pirabas Formation (Lower Miocene), Pará State, Brazil, vol. 37–2. Anuário do Instituto de Geociências – UFRJ, Rio de Janeiro, pp. 100–110 (ISSN: 0101-9759).

Thorburn, D.C., Morgan, D.L., Rowland, A.J., Gill, H.S., Paling, E., 2008. Life history notes of the Critically Endangered dwarf sawfish, *Pristis clavata*, Garman 1906 from the Kimberley region of Western Australia. Environ. Biol. Fish 83, 139–145.

Tschopp, H.J., 1953. Oil explorations in the Oriente of Ecuador. Am. Assoc. Pet. Geol. Bull. 37, 2303–2347.

Uba, C.E., Hasler, C.-A., Buatois, L.A., Schmitt, A.K., Plessen, B., 2009. Isotopic, paleontologic, and ichnologic evidence for late Miocene pulses of marine incursions in the Central Andes. Geology 37 (9), 827–830.

Urey, H.C., Lowenstam, H.A., Epstein, S., McKinney, C.R., 1951. Measurement of paleotemperatures and temperatures of the upper cretaceous of England, Denmark, and the southeastern United-States. Geol. Soc. Am. Bull. 62, 399–416.

Van Soelen, E.E., Kim, J.-H., Santos, R.V., Dantas, E.L., de Almeida, F.V., Pires, J.P., Roddaz, M., Damsté, J.S.S., 2017. A 30 Ma history of the Amazon River inferred from terrigenous sediments and organic matter on the Ceará Rise. Earth Planet Sci. Lett. [serial on the Internet] 474, 40–48. https://doi.org/10.1016/j.epsl.2017.06.025.

Varol, B., 2015. Stable isotopes of mollusk shells in environmental interpretations; an exemple from Sinop Miocene succession (Northern Turkey). Bull. Mineral Res. Explor. 128.

Veizer, J., 1983. Chemical diagenesis of carbonates: theory and application of trace element technique, Stable isotopes in sedimentary geology: society of economic paleontologists and mineralogists short course. Dallas 3, 1–3.100.

Venturieri, A., Watrin, O.S., Rocha, A.M.Á., Silva, B.N.R., 1998. Avaliação da dinâmica da paisagem da Ilha do Mosqueiro, Município de Belém, Pará. In: Simpósio Brasileiro de Sensoriamento Remoto, 9. (SBSR), 1998. INPE, São José dos Campos, pp. 247–256. ISBN: 85-17-00015-3.

Villegas, S.S., van Soelen, E.E., van Manen, M.L.T., Flantua, S.G.A., Santos, R.V., Roddaz, M., Dantas, E.L., van Loon, E., Damsté, J.S.S., Kim, J.-H., Hoorn, C., 2016. Amazon forest dynamics under changing abiotic conditions in the Early Miocene (Colombian Amazonia). J. Biogeogr. 43, 2424–2437. https://doi.org/10.1111/jbi.12769.

Vogel, J.C., Ehleringer, J.R., Hall, A.E., Farquhar, G.D., 1993. Variability of carbon isotope fractionation during photosynthesis. In: Stable Isotopes and Plant Carbon-Water Relations. Academic Press Inc, pp. 29–46.

Vonhof, H.B., Wesselingh, F.P., Ganssen, G.M., 1998. Recostruction of the Miocene Western Amazonian aquatic system using moluscan isotopes signatures. Palaeogeogr. Palaeoclimatol. Palaeoecol. 141, 85–93.

Vonhof, H.B., Wesselingh, F.P., Kaandorp, R.J.G., Davies, G.R., van Hinte, J.E., Guerrero, J., Räsänen, M., Romero-Pittman, L., Ranzi, A., 2003. Paleogeography of Miocene Western Amazona: isotopic composition of molluscan shells constrains the influence of marine incursions. Bull. Geol. Soc. Am. 115, 983–993. https://doi.org/10.1130/B25058.1.

Weiner, S., Dove, P.M., 2003. An over view of biomineralization processes and the problem of the vital effect. In: Dove, P.M., De Yoreo, J.J., Weiner, S. (Eds.), Biomineralization. Rev. Mineral. Geochem, 54, pp. 1–29.

Wesselingh, F.P., Macsotay, O., 2006. Pachydon hettneri (Anderson, 1928) as indicator for Caribbean-Amazonian lowland connections during the Early-Middle Miocene. J. S. Am. Earth Sci. 21, 49–53.

Wesselingh, F.P., Rasanen, M., Vonhof, H.B., Kaamdorp, R., Renema, W., Romero Pittman, L., Gingras, M., 2002. Lake Pebas: a palaeoecological reconstruction of a Miocene, long-lived lake complex in western Amazonia. Cainozoic Res. 1, 35–81.

Wesselingh, F.P., Kaandorp, R.J.G., Vonhof, H.B., Räsänen, M.E., Renema, W., Gingras, M., 2006. The nature of aquatic landscapes in the Miocene of western Amazonia: an integrated palaeontological and geochemical approach. Scr. Geol. 363–393.

Wesselingh, F.P., Hoorn, C., Kroonenberg, S.B., Antonelli, A.A., Lundberg, J.G., Vonhof, H.B., Hooghiemstra, H., 2010. On the origin of Amazonian landscapes and biodiversity: A synthesis. In: Hoorn, C., Wesseling, F.P. (Eds.), Amazonia, Landscape and Species Evolution. Wiley-Blackwell, Oxford, pp. 421–432.

Yeo, D.C.J., Ng, P.K.L., Cumberlidge, N., Magalhães, C., Daniels, S.R., Campos, M.R., 2008. Global diversity of crabs (Crustacea: Decapoda: Brachyura) in freshwater. Hydrobiologia 595 (1), 275–286.

Zalán, P.V., Matsuda, N.S., 2007. Bacia do Marajó. Boletim de Geociencias da Petrobras 15, 311–319.

Zmiri, A., Kaha, D., Hochstein, S., Reiss, Z., 1974. Phototaxis and thermotaxis in some species of *Amphistegina* (Foraminifera). J. Protozool. 21, 133–138.